IMPROVED FAULT DETECTION AND ISOLATION USING ENHANCED MULTISCALE PRINCIPAL COMPONENT ANALYSIS: ALGORITHMS AND APPLICATIONS

A Thesis

by

BYANNE QUTAIBAH MALLUHI

Submitted to the Office of Graduate and Professional Studies of
Texas A&M University
in partial fulfillment of the requirements for the degree of

MASTER OF SCIENCE

Chair of Committee,	Mohamed Nounou
Co-Chair of Committee,	Hazem Nounou
Committee Member,	Ahmed Abdel-Wahab
Head of Department,	Arul Jayaraman

December 2019

Major Subject: Chemical Engineering

ABSTRACT

Effective and reliable fault detection and isolation (FDI) methods are essential for the efficient operation of industrial processes. This work has developed a data-driven algorithm called Enhanced Multi-Scale PCA (EMSPCA) to improve fault detection performance of the conventional MSPCA method. It also extends EMSPCA to isolation by utilizing a PCA reconstruction based approach to improve the fault isolation performance.

A critical analysis presented in this work, shows that the conventional MSPCA detection rate is obstructed by its inaccurate predictions of detection thresholds. To address this issue, EMSPCA alters the way wavelet coefficients are processed in the training and testing data, such that, the predicted threshold is suitably tighter for smaller fault projections, which ensures a much better detection rate. A soft-thresholding technique is also implemented to ensure the false alarm rates remain low. Moreover, this research extends the EMSPCA method to account for isolation at multiple scales. Previous research has used contribution plot isolation approaches in the multiscale framework, but here, the reconstruction-based approach is employed. Reconstruction-based approaches suffer less from the smearing effect and can therefore achieve better isolation rates. Smearing occurs when one variable contaminates or "smears" another variable's contribution or isolation index to the point of misdiagnosis. The work will investigate how the multiscale PCA framework can minimize the amount of smearing to produce optimal isolation performance. It will also offer a comparison between contribution plot and

reconstruction based isolation performances, and present the impact of decimated and undecimated wavelet transforms on detection and isolation performances.

To obtain statistical and meaningful conclusions, a randomized synthetic linear model with an embedded shift-in-the-mean univariate fault is utilized. Monte Carlo simulations are used to evaluate the false alarm, detection rates, and isolation rates across all decomposition depths and a range of fault sizes. To further validate the algorithm and the FDI improvements it realizes, this work will utilize real data from a pilot distillation plant and two TEP units with a fabricated sensor fault embedded. These results will demonstrate the superior FDI performance of the EMSPCA reconstruction-based approach.

ACKNOWLEDGEMENTS

I would like to thank my committee and co-chair, Dr. Mohamed Nounou and Dr. Hazem Nounou, for their mentorship and support through the course of my research. Without them, this thesis would not have been possible. I would also like to thank my committee member, Dr. Ahmad Abdel-Wahab, for his valuable support throughout the Master's program.

I would also like to thank my parents, for their encouragement and unconditional love. I hope to make you proud one day with even greater achievements. And my siblings, for putting a smile on my face, and my grandmother and for her warm love and support.

CONTRIBUTORS AND FUNDING SOURCES

Contributors

The thesis committee which supervised this work consists of: the chair, Dr. Mohamed Nounou, from the Department of Chemical Engineering, the co-chair, Dr. Hazem Nounou, from the Department of Electrical Engineering, and the committee member, Dr. Abdel Wahab, from the Department of Chemical Engineering.

The data analyzed in Section 5 was provided by Dr. Khaled Elsaid. It was obtained from a pilot distillation plant in Texas A&M University at Qatar. All other work presented in this thesis was completed by the student independently.

Funding Sources

The first year of graduate studies was supported by a graduate fellowship from Texas A&M University at Qatar. The second year was supported by the Qatar National Research Fund (NPRP9-330-2-140). The content of this work are solely the responsibility of the authors and do not necessarily represent the official views of QNRF.

NOMENCLATURE

FDI	Fault Detection and Isolation
MSPCA	Multiscale Principal Component Analysis
EMSPCA	Enhanced Multiscale Principal Component Analysis
PCA	Principal Component Analysis
CD	Complete Decomposition
RB	Reconstruction Based
PC	Principal Component
TEP	Tennessee Eastman Process
MC	Monte Carlo
DWT	Discrete Wavelet Transform
UWT	Undecimated Wavelet Transform
MS	Multiscale
FAR	False Alarm Rate
DR	Detection Rate
ST	Soft Thresholding
PB	Packed Bed
PP	Pilot Plant

TABLE OF CONTENTS

Page

LIST OF FIGURES

Page

LIST OF TABLES

Page

1. INTRODUCTION

1.1. Overview

Data analytics has gained a lot of interest in the field of process monitoring and control because of its ability to extract actionable information about the state of a process in real time [1]. Business leaders of big companies like BASF, Shell, and DOW are investing in Big Data technology, because they recognize the business value it can yield [2]. An estimated 20 billion dollars is lost every year by US petrochemical industries due to inadequate "abnormal situation management" [3], and this cost can be reduced by developing automated data-techniques that can accurately and reliably perform fault detection and isolation (FDI). Effective FDI methods help prevent costly situations resulting from delayed detections or erroneous isolations, which will warrant a safe and efficient operation of chemical plants [4].

The work will improve fault detection by modifying a well-established detection algorithm called, Multiscale Principal Component Analysis (MSPCA), and it will improve fault isolation by extending the developed algorithm to a reconstruction-based isolation approach.

Data-driven FDI algorithms, unlike model-based or expert-knowledge based algorithms, use only historical process data to build models [5]. Many data-driven algorithms are based on Principal Component Analysis (PCA) because of its ability to capture the correlation structure of historical data in a single model. With this model, PCA projects data into a modeled subspace, called principal component subspace, and an un-

modeled subspace, called residual subspace [6]. By computing various PCA detection and isolation indices, one can detect the fault and isolate the process variable that caused it. PCA FDI performance is compromised when the data is nonlinear, dynamic, Gaussian, and/or does not contains a moderate level of noise. As a result, several extensions of PCA, such as, kernel PCA, multiscale PCA (MSPCA), and exponentially weighted PCA have been developed [7] [8] [9].

The MSPCA formulation is highly effective in extracting information from process data that is nonlinear in nature and that consists of many contributing features such as noise, process dynamics, disturbances, etc. [8]. It utilizes the advantages of wavelet-based multiscale analysis to effectively separate stochastic and deterministic features and decorrelate auto-correlated signals, which improve the monitoring quality of PCA [10]. Several works have demonstrated the large improvements in MSPCA fault detection [11] [12] [13] [14] [15]. However, at times, the conventional way of carrying out MSPCA leads to unsuccessful detection even for *linear* data sets. One such example is illustrated by Zhang who highlights the inaccuracy of the coefficient selection step in the conventional MSPCA algorithm [16]. To the best of the author's knowledge, no work has thoroughly investigated the robustness of the conventional MSPCA algorithm for linear data sets. Therefore, the first objective of this work is to investigate this issue and accordingly suggest an Enhanced MSPCA (EMPCA) algorithm for improved fault detection. This issue will be investigated and discussed in Section 2 of the thesis.

MSPCA has been extended to improve fault isolation by works of Yoon and MacGregor in 2001 and Misra et. al. in 2004. Both of these methods rely on the complete

decomposition (CD) technique also known as contribution plots, and they illustrate how to diagnose the type of fault from its blueprint representation at multiple scales [5] [6]. However, the CD isolation method suffers from a phenomena called the "smearing effect" which can result in false isolations [18]. Another isolation technique called the reconstruction-based (RB) method, established in 2008, suffers less from smearing and is found to outperform the conventional CD method [19]. Alcala et al. extensively analyzes the smearing effect in both the CD and the RB methods and concludes that the RB approach can guarantee correct fault isolation for large enough faults while the CD method cannot [20]. Therefore, the second objective of this work is to improve EMSPCA-isolation by developing a new technique that utilizes the reconstruction based contribution method. This will be explored in Section 3 of the thesis.

Furthermore, this work will explore the advantages of using the undecimated or stationary wavelet transform over the commonly used decimated wavelet transform in the overall FDI performance. The decimated wavelet transform reduces the number of samples by half at each subsequent coarser scale to remove redundancy, while the undecimated wavelet transform does not [21]. This work will illustrate how data redundancy could be an advantage for data-driven techniques that require large sets of data to build models.

The remainder of this thesis is divided into five main sections: Section 2, which proposes the EMSPCA algorithm and investigates the detection performance; Section 3, which extends EMSPCA to RB isolation and investigates isolation performance; Section 4, which presents TEP unit application; Section 5, which presents a pilot-plant application

of the proposed FDI algorithm; and finally Section 6, which concludes the findings of this work and proposes future directions.

1.2. Research Contributions

The main contribution of this work is the development of an EMSPCA FDI algorithm that improves fault detection and fault isolation. The individual research objectives are listed as follows:

- Conduct an extensive analysis on the detection performance of the conventional MSPCA method to highlight the drawback in its threshold estimation.
- Propose a novel EMSPCA method that improves threshold estimation and thereby improves detection performance.
- Investigate the effects of fault size and decomposition depth on detection and isolation performance using Monte Carlo simulations of a simulated example.
- Investigate the effects of using the decimated and undecimated multiscale wavelet transforms on both the detection and isolation performances.
- Extend EMSPCA to reconstruction based isolation and compare it with EMSPCA contribution plot isolation.
- Test the EMSPCA FDI algorithm on experimental data obtained from a pilot distillation plant.
- Test the EMSPCA FDI algorithm on the stripper and separator TEP units.

2. IMPROVING FAULT DETECTION WITH EMSPCA

2.1. Introduction

Fault detection and isolation (FDI) are the process monitoring control tasks that ensure variables remain within their safe and normal limits. This section will address *fault detection* and the Enhanced Multi-Scale PCA (EMSPCA) algorithm will be introduced to improve the fault detection performance of the conventional MSPCA algorithm.

MSPCA combines the feature extraction quality of wavelet analysis with the monitoring quality of PCA to improve detection quality[8]. It was originally developed by Bakshi in 1998, and has proven to be highly effective for dynamic process data [10] [11] [12]. However, Zhang's work highlights that MSPCA can lead to poor detection performance for even linear data [16]. This section will further investigate when and why poor detection occurs when using the conventional MSPCA method. Accordingly, the Enhanced MSPCA algorithm will be proposed to tackle the drawbacks identified with MSPCA which improve the overall detection performance. This section will also demonstrate the effect of using decimated and undecimated wavelet transforms on the detection rates.

The upcoming subsections 2.2, 2.3, and 2.4 will provide a brief overview of PCA-based fault detection, multiscale analysis, and the conventional MSPCA algorithm. Section 2.5 will present an extensive analysis of MSPCA detection performance and the motivation for EMSPCA, followed by Section 2.6, which will discuss the EMSPCA algorithm and the results. Section 3 will extend the developed algorithm to improve fault

isolation. Section 4 and 5 will test the proposed algorithm on two different applications, the TEP and the pilot distillation plant.

2.2. PCA Detection

PCA transforms the original process variables to a new set of variables called principal components (PC). The first PC is in the direction which captures the highest variability in the data, and every succeeding principal component captures the highest remaining variability. The principal components are orthogonal to each other and represent a new basis for the data [22].

PCA is oftentimes called a *dimension reduction technique* because of its ability to reduce the dimensionality of the data by removing the principal components which capture the lowest variability [8]. For example, consider Figure 1, which shows x-y data as red dots and their corresponding principle directions as blue arrows, labeled v1 and v2. The first PC (v1), which captures the important variability, is used to model the data, while the second PC (v2), which captures the variations due to noise, is discarded as residuals.

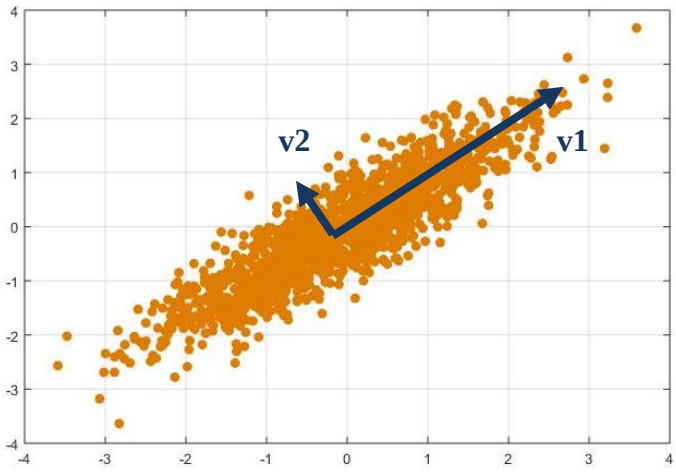

Figure 1: Simple PCA visual.

PCA is a powerful technique when it comes to dealing with many variables (high dimensions) because it can capture the underlying correlations and removes the noise. A typical chemical process has a large set of variables that are correlated due to the physical laws governing them. This makes PCA highly valuable in extracting useful information and using it to detect and isolate faults in chemical processes [23].

The PCA model is constructed using non-faulty historical process data that are assumed to contain all possible variabilities. Let $\boldsymbol{X} \in \mathbb{R}^{m \times n}$ be a data matrix with dimensions $m \times n$ (m variables and n observations). Each variable is normalized to zero mean and unit standard deviation. The first step in PCA is to perform an eigen-decomposition on the covariance matrix $\boldsymbol{R}$, which gives [24],

$$\boldsymbol{R} \equiv \frac{\boldsymbol{X}\,\boldsymbol{X}^{\boldsymbol{T}}}{n-1} = \boldsymbol{P}\,\boldsymbol{\Lambda}\,\boldsymbol{P}^{\boldsymbol{T}} \quad (m \times m).$$

The columns ($\boldsymbol{p}_i$) of the $\boldsymbol{P}$ matrix are the orthogonal eigenvectors (or loading vectors) of the covariance matrix $\boldsymbol{R}$, and the diagonal elements of the matrix $\boldsymbol{\Lambda}$ are the corresponding eigenvalues (λ_i). Each $\boldsymbol{p}_i$ represents a direction that captures some variation in the data, and the corresponding λ_i quantifies the amount of variation captured [25]. A key feature in PCA is determining the number of loading vectors to retain (l). The retained loading vectors (or principal components- PC's) capture the underlying variations in the data, while the discarded PC's represent only the noise variations. An l value that is too high or too low can jeopardize the accuracy of the model [6]. Consequently, there are several techniques for determining l in literature; the Scree test [25], cross validation [26][27], and cumulative percent variance CPV [13] are among the most commonly used methods.

The PCA process model $\boldsymbol{C}$ is computed by [24],

$$\boldsymbol{C} = \widehat{\boldsymbol{P}}\widehat{\boldsymbol{P}}^{\boldsymbol{T}},$$

where $\widehat{\boldsymbol{P}}$ are the retained loading vectors in an $(m \times l)$ matrix**.** The PCA model decomposes the data matrix $\boldsymbol{X}$**,** into modeled data, $\widehat{\boldsymbol{X}}$, and unmodeled data (or residual data), $\widetilde{\boldsymbol{X}}$ [23],

$$\boldsymbol{X} = \widehat{\boldsymbol{X}} + \widetilde{\boldsymbol{X}} \qquad \boldsymbol{X} \in \mathbb{R}^{m \times n},$$

where,

$$\widehat{\boldsymbol{X}} = \boldsymbol{C}\boldsymbol{X} \text{ and } \widetilde{\boldsymbol{X}} = (\boldsymbol{I} - \boldsymbol{C})\boldsymbol{X} \text{ [24]}.$$

The matrices $\boldsymbol{C}$ and $\boldsymbol{I} - \boldsymbol{C}$ are transformations which project the data onto a principal component space (PCS) and a residual subspace (RS) as illustrated in Figure 2 adapted from [23]. The addition of the two, completes the measurement space.

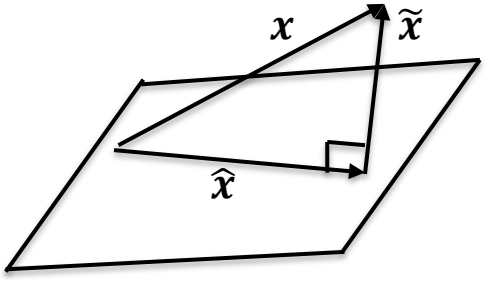

Figure 2: The principal component projections (adapted from [23]).

Fault detection using the PCA model can be carried out using three fault detection indices that will be described next.

2.2.1. PCA Detection Statistics

There are three common fault detection indices associated with PCA: Q, T^2, and, φ. A detection statistic and a detection threshold, can be used to indicate how likely a fault has occurred. Usually, a detection statistic the crosses a threshold is highly likely to be faulty and so is flagged as a fault. For a single sample, and of the PCA detection statistics can be computed by the general equation [28],

$$index(\boldsymbol{x}) = \boldsymbol{x}^T \boldsymbol{M} \boldsymbol{x} = \left\| \boldsymbol{M}^{\boldsymbol{1/2}} \boldsymbol{x} \right\|^2$$

where $\boldsymbol{M}$ can represent any of the fault detection statistics summarized in Table 1 [29].

Table 1: General M index for fault detection [29]

index	SPE/Q	T^2	φ
M	$\boldsymbol{I - C}$	$\widehat{\boldsymbol{P}}\widehat{\boldsymbol{\Lambda}}^{-1}\widehat{\boldsymbol{P}}^{\boldsymbol{T}}$	$\boldsymbol{\Phi} = \frac{\widehat{\boldsymbol{P}}\widehat{\boldsymbol{\Lambda}}^{-1}\widehat{\boldsymbol{P}}^{\boldsymbol{T}}}{\tau^2} + \frac{\widetilde{\boldsymbol{C}}}{\delta^2}$

The Q statistic detects the faults which appear in the residual subspace, and the T^2 statistic detects the faults which appear in the principal component subspace [23]. The combined index (φ) combines the effects of both the Q and the T^2 statistics, thus, providing a complete measure of variability in the entire space. This work will utilize the Q statistic in its analysis because the residual space can capture a wide range of abnormal conditions that cause a disruption in the correlation structure of the data. The Q statistic's sensitivity towards the correlation structure is advantageous because relatively small faults can be captured [30].

2.2.1.1. Q Statistic

The Q statistic is often called the square prediction error (SPE) and is defined by [31],

$$Q(\boldsymbol{x}) = \boldsymbol{x}^T \boldsymbol{M} \boldsymbol{x} = \boldsymbol{x}^T (\boldsymbol{I} - \boldsymbol{C}) \boldsymbol{x} = \left\| (\boldsymbol{I} - \boldsymbol{C})^{\frac{1}{2}} \boldsymbol{x} \right\|^2 = \|\boldsymbol{x} - \hat{\boldsymbol{x}}\|^2 = \|\tilde{\boldsymbol{x}}\|^2.$$

It represents the sum of squared errors between the original data ($\boldsymbol{x}$) and the modeled data ($\hat{\boldsymbol{x}}$).

The confidence limit (δ^2) for the SPE was originally developed by Jackson and Mudholker under the assumption that the residuals follow a normal distribution [32]. By a second order moment approximation, the confidence limit is calculated by [29],

$$\delta^2 = \frac{\theta_2}{\theta_1} \chi_\alpha^2 \left(\frac{\theta_1^2}{\theta_2} \right)$$

where α is the confidence limit, $\theta_1 = \sum_{i=l+1}^{m} \lambda_i$, $\theta_2 = \sum_{i=l+1}^{m} \lambda_i^2$, and λ_i are the eigenvalues. The detection limit can also be obtained empirically for residuals that do not follow a normal distribution. When $Q(\boldsymbol{x}) \geq \delta^2$, an error is flagged, which indicates that

there occurred a breakdown in the correlation structure among variables due to a potential fault [29]. The Q statistic captures a large variety of faults, and it will be used in all the analysis/results presented in this work.

2.2.1.2. T^2 Statistic

The T^2 statistic measures the variations of the scores and was originally developed by Hoteling 1933 [33]. The T^2 index at any time sample is computed by [29],

$$T^2(\boldsymbol{x}) = \boldsymbol{x}^T \boldsymbol{M} \boldsymbol{x} = \boldsymbol{x}^T \widehat{\boldsymbol{P}} \widehat{\boldsymbol{\Lambda}}^{-1} \widehat{\boldsymbol{P}}^T \boldsymbol{x} = \left\| \left(\widehat{\boldsymbol{P}} \widehat{\boldsymbol{\Lambda}}^{-1} \widehat{\boldsymbol{P}}^T \right)^{1/2} \boldsymbol{x} \right\|^2$$

where $\widehat{\boldsymbol{P}}$ is the retained principal components and $\widehat{\boldsymbol{\Lambda}}$ is the diagonal matrix of the eigenvalues associated with them. The index represents the sum of the squared scores. When the T^2 index exceeds a certain control limit ($T^2(\boldsymbol{x}) \geq \tau^2$), an error is flagged.

The T^2 statistic control limit can be computed empirically from data representing normal operation (i.e., the training data). However, it can also be computed statistically by a chi-distribution, $\tau^2 = \chi_\alpha^2(l)$ with a confidence level α, or by an F-distribution, $\tau^2 = \frac{(n^2-1)\alpha}{n(n-1)} F_\alpha(l, n-l)$, where l and $n-l$ degrees of freedom of the F-distribution [29] [34]. The T^2 helps identify another kind of abnormal condition where the operating variability is out of range. Since the T^2 index flags an error when there is a change of variance, it requires a relatively large fault to be noticed [29].

2.2.1.3. φ Statistic

The combined index φ, was proposed by Yue and Qin, and it is a combination of the T^2 and Q statistic and it is computed by [35],

$$\varphi(\boldsymbol{x}) = \boldsymbol{x}^T \boldsymbol{M} \boldsymbol{x} = \boldsymbol{x}^T \boldsymbol{\Phi} \boldsymbol{x} = \left\| \boldsymbol{\Phi}^{1/2} \boldsymbol{x} \right\|^2$$

where,

$$\boldsymbol{\Phi} = \frac{(\mathbf{I} - \mathbf{C})}{\delta^2} + \frac{\widehat{\boldsymbol{P}}\widehat{\boldsymbol{\Lambda}}^{-1}\widehat{\boldsymbol{P}}^{\boldsymbol{T}}}{\tau^2}.$$

The statistical control limit is obtained by [35],

$$\zeta^2 = \frac{\left(\frac{1}{\tau^4} + \frac{\theta_2}{\delta^4}\right)}{\left(\frac{1}{\tau^2} + \frac{\theta_1}{\delta^2}\right)} \chi_\alpha^2 \left(\frac{\left(\frac{1}{\tau^2} + \frac{\theta_1}{\delta^2}\right)^2}{\left(\frac{1}{\tau^4} + \frac{\theta_2}{\delta^4}\right)} \right)$$

where τ^2 and δ^2 are the confidence limit for the T^2 and Q statistics, $\theta_1 = \sum_{i=l+1}^{m} \lambda_i$, $\theta_2 = \sum_{i=l+1}^{m} \lambda_i^2$, and λ_i are the eigenvalues. When an error is flagged, the combined index can indicate a fault which caused an abnormal variation within the scores and/or a breakdown of the correlation structure.

2.2.2. Detectability Conditions

The detectability conditions are a set of conditions, which when satisfied, guarantee a fault detectable (i.e. the statistic will cross the limit). This section will demonstrate the detectability conditions for the Q statistic specifically as it will be used throughout this work. Assume a data sample is divided into the non-faulty and the faulty components as follows,

$$\boldsymbol{x} = \boldsymbol{x}^* + f\boldsymbol{\xi_i},$$

where $\boldsymbol{x}^*$ is the non-faulty component, and $f\boldsymbol{\xi_i}$ represents the faulty component's magnitude and direction. The residual projection of the above equation yields,

$$\tilde{\boldsymbol{x}} = \tilde{\boldsymbol{x}}^* + f\tilde{\boldsymbol{\xi}}_{\boldsymbol{i}}$$

It is necessary that a fault direction *exists* in the residual space, i.e. $\tilde{\boldsymbol{\xi}}_{\boldsymbol{i}} \neq \mathbf{0}$, otherwise no fault can be observed and detection cannot occur.

To guarantee fault detection, the magnitude of the fault projection should satisfy a minimum in order to exceed the detection threshold. This is illustrated by normalizing the fault direction, $\tilde{\boldsymbol{\xi}}_{\boldsymbol{i}} = \|\tilde{\boldsymbol{\xi}}_{\boldsymbol{i}}\|\tilde{\boldsymbol{\xi}}_{\boldsymbol{i}}^{\boldsymbol{o}}$, and re-writing the above equation as,

$$\tilde{\boldsymbol{x}} = \tilde{\boldsymbol{x}}^{*} + f\|\tilde{\boldsymbol{\xi}}_{\boldsymbol{i}}\|\tilde{\boldsymbol{\xi}}_{\boldsymbol{i}}^{\boldsymbol{o}} = \tilde{\boldsymbol{x}}^{*} + \tilde{f}\tilde{\boldsymbol{\xi}}_{\boldsymbol{i}}^{\boldsymbol{o}},$$

where the term, $\tilde{f}$ represents the fault magnitude projected in the residual space. A fault is guaranteed detectable when this orthogonal distance is larger than the diameter of the confidence region (2δ) [6],

$$|\tilde{f}| > 2\delta.$$

This was a result of derivation provided by [6]. This suggests the importance of considering the "fault projection" rather than the actual fault size for Q statistic detection.

2.3. Multiscale Analysis

PCA detection performs well under the assumptions of independent Gaussian noise at moderate levels [36]. Multiscale analysis will help address violations in these assumptions by enabling effective feature extraction and decorrelation of autocorrelated signals, which improve the overall detection performance.

The main advantage behind wavelet-based multiscale analysis is the ability to view a function or a signal at multiple scales that are localized in both time and frequency. This analysis is useful for real process data which contain multiple features (such as process dynamics and measurement noise) that appear more prominently in specific scales. Some of the multiscale representation algorithms -the decimated and undecimated wavelet transforms- are described in this Section.

2.3.1. Decimated Wavelet Transforms

A decimated wavelet transform (DWT) is the projection of a signal onto a set of orthonormal basis functions, called the wavelet and scaling functions [37]. Well-known examples of wavelet functions include the Haar, Daubechies, Coiflet, and Symlet functions [38]. This work will use the wavelet Haar for its simplicity and the effectiveness of using other wavelets may be considered for future work. All wavelet functions are defined with a set of dilations and translations as shown by [8],

$$\psi_{sk}(t) = \frac{1}{\sqrt{s}}\psi\left(\frac{t-k}{s}\right),$$

where s is the dilation parameter that determines the scale, and k is the translation parameter that determines the shift in time [8]. The scaling and translation parameters are manipulated to facilitate the multiresolution wavelet analysis. For practical purposes, when dealing with discrete signals, the wavelet and scaling functions can be discretized dyadically with the dilation parameter as $s = 2^j$ [8],

$$\psi_{jk}(t) = \frac{1}{\sqrt{2^j}}\psi\left(\frac{t-2^j k}{2^j}\right),$$

Each wavelet function has a corresponding orthonormal scaling function with a similar formula,

$$\varphi_{jk}(t) = \frac{1}{\sqrt{2^j}}\varphi\left(\frac{t-2^j k}{2^j}\right).$$

The DWT can be implemented by convoluting a signal with filter bank structure with low pass and high pass filters, which are derived from the scaling and wavelet functions respectively [37]. Thus a wavelet decomposition uses, a high pass filter, with

impulse response g derived from the wavelet functions $\psi(t)$, and a low pass filter, with impulse response h derived from the scaling function $\varphi(t)$ [39]. An algorithm for implementing the DWT was first developed by Mallat in 1989 [40]. His algorithm relies on the application of the filters h and g and the down-samplers ($\downarrow 2$), over and over on the approximate scale output as illustrated in Figure 3. This figure is an edited version of a figure found in [41].

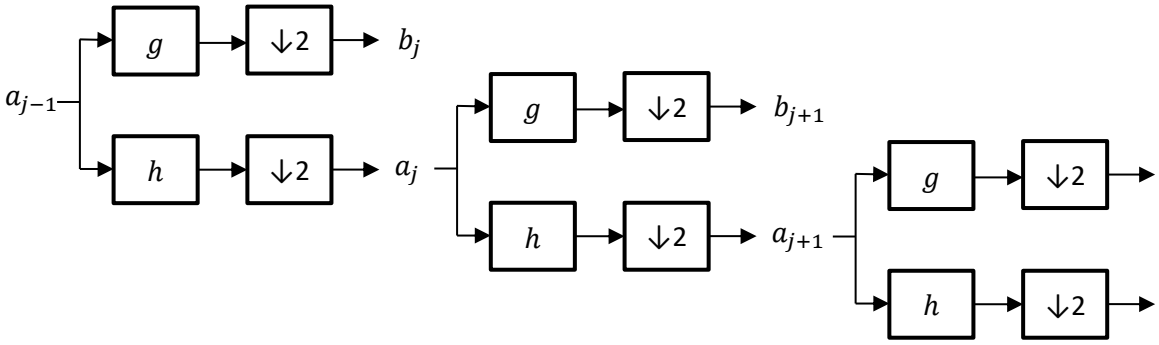

Figure 3: Schematic diagram of the decimated wavelet transform (adapted [41]).

The DWT algorithm illustrated in Figure 3 shows, that given a time-domain signal, a_{j-1}, a coarser approximation of the signal, called the first scaled (or approximate) signal, **a_1,** can be computed by convoluting the signal with the low pass filter *h*. The difference between the time-domain signal and the first scaled signal can be computed by convoluting the time-domain signal with the high pass filter, *g*, and is called the first detail signal. This process can be repeated using the first scaled signal to get the second scaled and detail signals, **a_2** and **b_2**, respectively. Refer to Figure 4 for the visual illustration.

Repeating this process J times, the signal can be represented as the sum of all detail signals at all scales and the last scaled signal as follows:

$$x(t) = \sum_{k=1}^{N2^{-J}} a_{Jk}\varphi_{Jk}(t) + \sum_{j=1}^{J}\sum_{k=1}^{K} b_{jk}\psi_{jk}(t)$$

where a_{JK} and b_{jk} are the approximate and detail coefficients corresponding to the scaling $\varphi_{jk}(t)$ and wavelet $\psi_{jk}(t)$ functions; J represents the decomposition depth ranging between 1 and $\log_2(N)$, where N is the signal length; and K is the translation parameter ranging from 1 to $N2^{-j}$. This equation shows how a signal can be decomposed into multiple scales and likewise how it can be reconstructed back to the time domain.

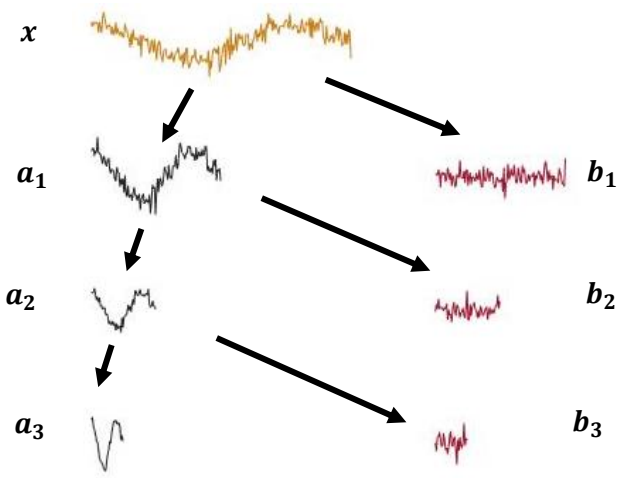

Figure 4: Decimated wavelet decomposition of a signal at multiple scales.

The DWT can also be computed using matrix multiplication by multiplying a signal $\boldsymbol{x}$ (represented as $(N \times 1)$ column vector) by a matrix $\boldsymbol{W}$ as follows [38],

$$x_w = \boldsymbol{W}x$$

where, x_w $(N \times 1)$ contains the final approximate scale coefficients and all the detailed coefficients, and $\boldsymbol{W}$ is the $(N \times N)$ filter matrix. The filter matrix ($\boldsymbol{W}$) has the high pass and low pass filter coefficients organized in a specific way depending on the size of the time-domain signal (N) and the decomposition depth (J) [8][14]. When decomposing to the maximum possible depth (i.e. $J = \log_2(N)$), $\boldsymbol{W}$ takes the following form,

$$\boldsymbol{W} = \begin{bmatrix} h_{J,1} & h_{J,2} & \cdots & \cdots & \cdots & \cdots & \cdots & \cdots & \cdots & h_{J,N} \\ g_{J,1} & g_{J,2} & \cdots & \cdots & \cdots & \cdots & \cdots & \cdots & \cdots & g_{J,N} \\ g_{J-1,1} & g_{J-1,2} & \cdots & \cdots & g_{J-1,\frac{N}{2}} & 0 & 0 & \cdots & \cdots & 0 \\ 0 & 0 & \cdots & \cdots & 0 & g_{J-1,\frac{N}{2}+1} & g_{J-1,\frac{N}{2}+2} & \cdots & \cdots & g_{J-1,N} \\ \ddots & \ddots & \ddots & \ddots & \ddots & \ddots & \ddots & \ddots & \ddots & \ddots \\ \ddots & \ddots & \ddots & \ddots & \ddots & \ddots & \ddots & \ddots & \ddots & \ddots \\ g_{1,1} & g_{1,2} & 0 & 0 & \cdots & \cdots & \cdots & \cdots & \cdots & 0 \\ \ddots & \ddots & \ddots & \ddots & \ddots & \ddots & \ddots & \ddots & \ddots & \ddots \\ 0 & 0 & \cdots & \cdots & \cdots & 0 & g_{1,N-3} & g_{1,N-2} & 0 & 0 \\ 0 & 0 & \cdots & \cdots & \cdots & \cdots & \cdots & 0 & g_{1,N-1} & g_{1,N} \end{bmatrix}$$

where $h_{j.n}$ and $g_{j,n}$ are the filter coefficients with subscripts j and n representing the scale and sample number.

Some of the significant issues that arise from down-sampling include: 1) the number of samples is halved at every ensuing scale, which is an issue if large data sets are needed , and 2) it makes the DWT time-variant, i.e., the location of a feature in time will affect its representation at multiple scales. These issues are resolved by the stationary wavelet transform, which is discussed in the next section.

2.3.2. Undecimated Wavelet Transform

The main difference between the DWT and the undecimated (or stationary) wavelet transform (UWT) is that UWT does not involve down-sampling, and thus, the

same number of samples is maintained at every scale. This can be an advantage for data-driven techniques that require large data sets for statistical inference [41]. Secondly, the time-variant concern is no longer applicable in stationary wavelet transform. UWT can be implemented using application of low pass and high pass filters as shown in Figure 5, which is an adaptation from the a figure in [41].

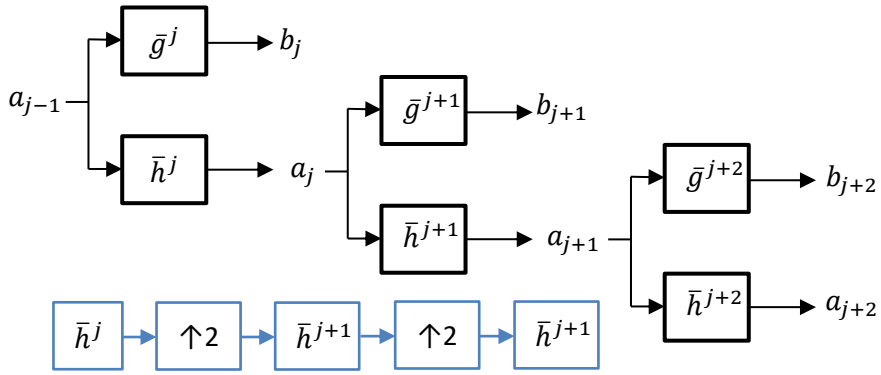

Figure 5: Schematic diagram of the undecimated wavelet transform (adapted [41]).

As Figure 5 indicates, the UWT does not down-sample the scaled or detail signals, instead, it up-samples the low pass and high pass filters at every subsequent coarser scale. This allows the lengths of the scaled and detail signals to maintain the same at all scales (see Figure 6). Note that UWT can also be performed for a signal represented by multiplying a vector x with a matrix $\boldsymbol{W_u}$ (of size $(J+1)N \times N$), which gives a vector of size $(J+1)N \times 1$, containing the scaled signal and all detail signals. The SWT of a signal is illustrated in Figure 6.

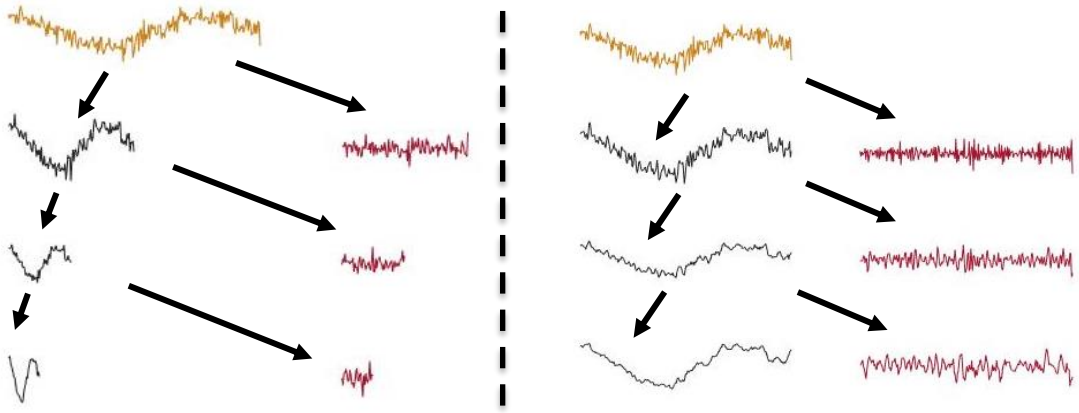

Figure 6: Decimated (left) and undecimated (right) wavelet decompositions.

The decimated and the undecimated wavelet decompositions involve transforming the data into different scales, which sets up the framework for MSPCA. To reconstruct the decomposed signals back to the time domain, all detail scales and only the final approximate scale are required. Therefore, only those scales will be involved in the MSPCA algorithm. The next section will describe the conventional MSPCA algorithm which integrates PCA at every scales.

2.4. MSPCA Detection Algorithm

The conventional MSPCA algorithm was originally published in 1998 by Bakshi [8], and its steps are summarized in the flow chart below.

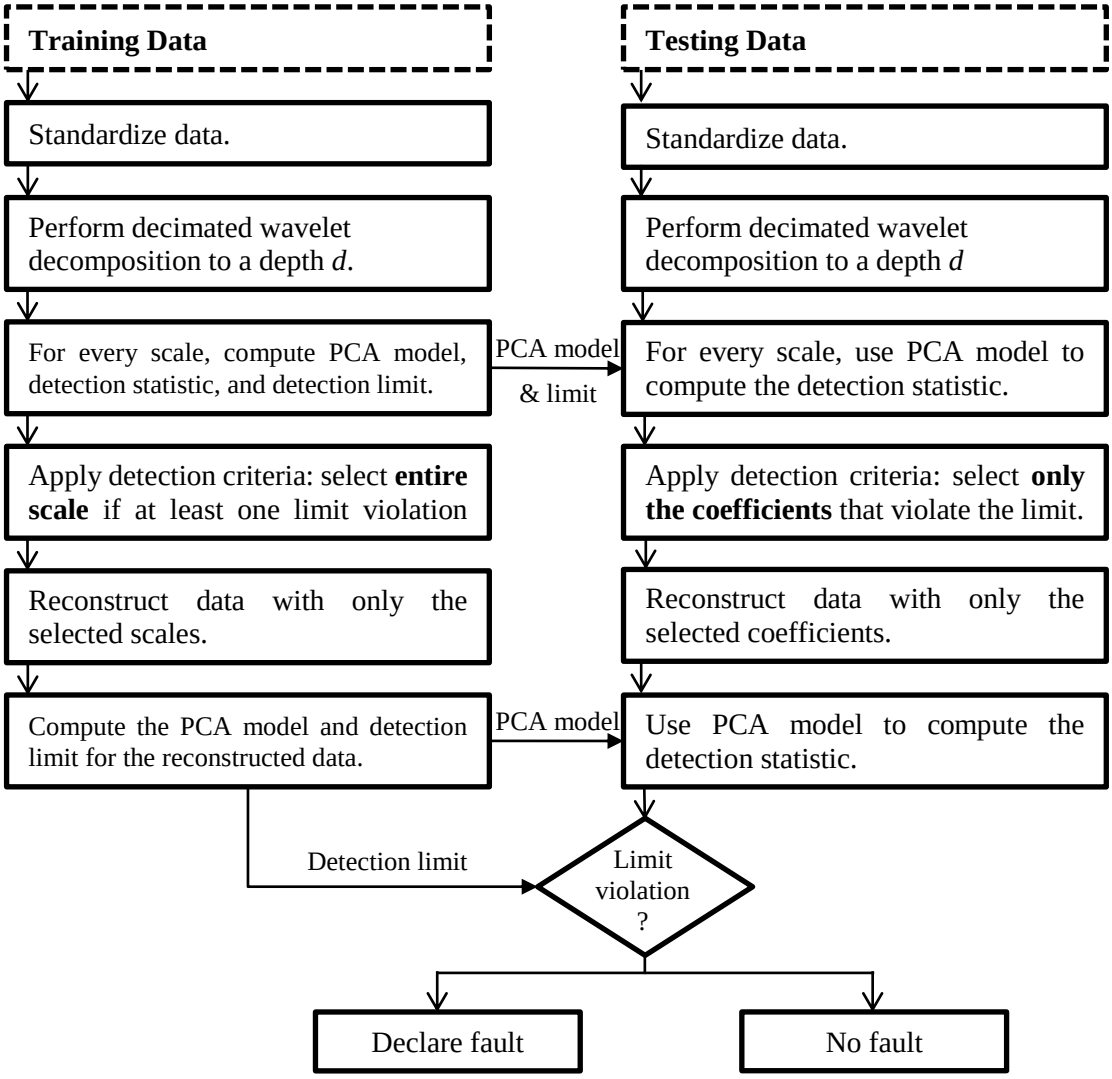

Figure 7: Conventional MSPCA algorithm in a flowchart.

As shown in Figure 7, the first step is to standardize the data to unit variance and zero mean. Then, the decimated wavelet transform is used to decompose the training and testing data to a depth *d*, which produces *d* detail scales and one approximate scale. For every scale derived from the *training data*, a PCA model and a detection threshold or limit is determined and stored to be used in every scale derived from the *testing data*. The PCA

models are used to compute the detection statistics for every scale. Then, a detection criteria is used to process the training and testing signals; in the *training data*, when one detection violation occurs (i.e., the detection statistic crosses the threshold), the entire scale is retained for reconstruction. However, in the *testing data*, only the coefficients that violate the limit are retained for reconstruction.

The selected scales/coefficients are reconstructed back to the time domain with the inverse decimated wavelet transform. The reconstructed training data is used to compute a new PCA model and a new detection limit that are applied to the testing data to detect faults in real time. In the upcoming sections, the MSPCA algorithm, will be implemented and analyzed. The conducted analysis will motivate the development of the modified version called enhanced MSPCA (EMSPCA).

2.5. Motivating Example

This section investigates the detection performance of the MSPCA algorithm for a linear data set with a univariate bias fault. Detection performance is evaluated by detection and false alarm rates. A randomized synthetic model and Monte Carlo simulations are used to obtain meaningful and un-bias conclusions. Through which, a histogram distribution of the detection rates and the relationship between detection threshold values and fault projections will be analyzed. This analysis will explain the drawbacks of the conventional MSPCA method which will motivate enhancing its performance by modifications in the algorithm.

2.5.1. Process Model and Simulation Conditions

The process model used to analyze the performance of the MSPCA algorithm has the following form,

$$\begin{bmatrix} x_1 \\ x_2 \\ x_3 \\ x_4 \\ x_5 \\ x_6 \end{bmatrix} = [M] \begin{bmatrix} t_1 \\ t_2 \\ t_3 \end{bmatrix} + noise$$

where, $x_1, x_2, \ldots x_6$ represent process variables that are functions of, $t_1 \sim 1N(0,1)$, $t_2 \sim 0.8N(0,1)$, and $t_3 \sim 0.6N(0,1)$. Zero-mean measurement noise that follows the distribution, $noise \sim 0.2N(0,1)$, is added to all variables, and M is a 6×3 matrix where its elements are generated from a $N(0.2, 1)$ distribution. Note that the model changes in every Monte Carlo run, to ensure that the results are not bias towards a single model structure. Some of the important conditions that are used in the analysis are listed below:

- Theoretical limits with 99% and 98% confidence levels are used, the first is used for detail signal thresholding, and the latter for the reconstructed signal detection. The confidence level values are recommended by the original MSPCA work[8].
- The number of retained principal components is 3.
- At every iteration the fault location is randomized and the process model is generated randomly.
- The number of Monte Carlo realizations is 3000.

2.5.2. Simulations Results

The performance of the MSPCA is evaluated by two metrics: the detection rate and false alarm rate. The detection rate (DR) is an indication of how well a method can correctly identify the presence of a fault and it is defined by, $DR =$

$\frac{number\ of\ detected\ faulty\ samples}{total\ number\ of\ faulty\ samples} * 100$. The false alarm rate (FAR) is an indication of a type 1 error, that is, when a sample is falsely indicated as a fault when it is not, and it is defined by, $FAR = \frac{number\ of\ \boldsymbol{detected\ nonfaulty}\ samples}{total\ number\ of\ nonfaulty\ samples} * 100$.

The DR and FAR as functions of the decomposition depths used in the MSPCA technique are plotted in the Figure 8.

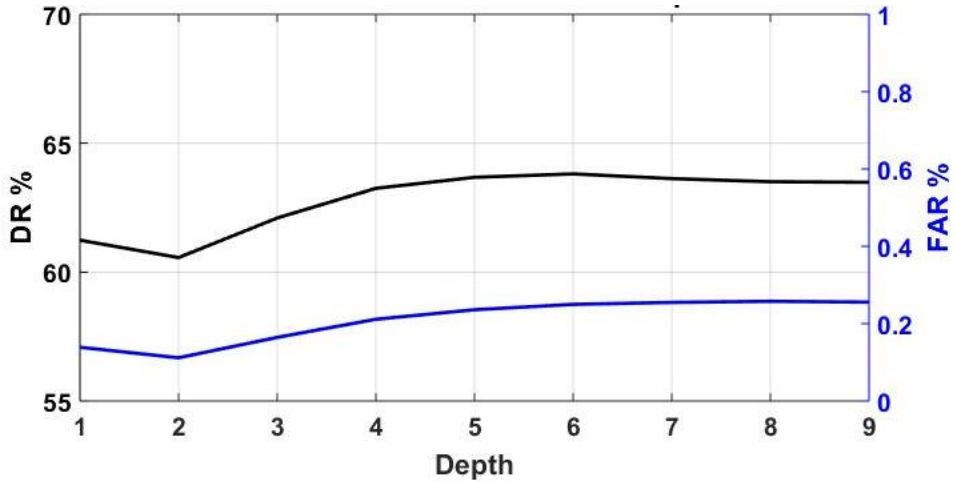

Figure 8: MSPCA detection performance across 9 decomposition depths.

As can be seen from Figure 8, the MSPCA method suffers from a low DR (that averages around 63%) but at the same time has a favorable FAR (that averages around 0.2%). To further analyze the low DR, a histogram plot showing the distribution for a decomposition depth of 4 was generated as shown in Figure 9.

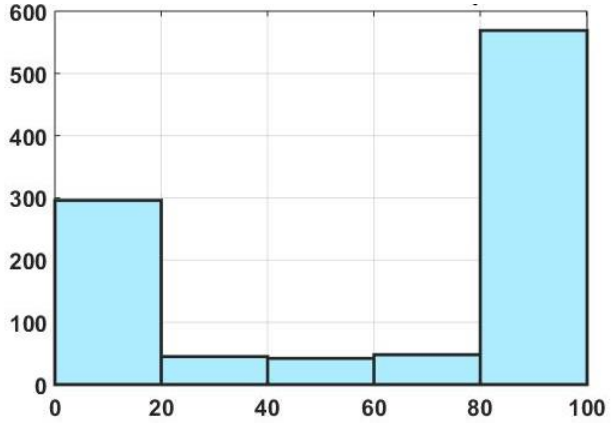

Figure 9: MSPCA DR histogram distribution for depth 4.

As can be seen from Figure 9, the detection completely fails (i.e. a DR below 20%) for a substantial number of cases (Monte Carlo realizations). Hence, the high count of unsuccessful detection is a major drawback of the conventional MSPCA method.

As stated earlier, a fault is guaranteed detectable when the condition, $|\tilde{f}| > 2\delta$, is met (where $\tilde{f}$ is the fault projection and δ is the square-root of the threshold value). Hence, successful detection is determined by an interplay of two factors: (1) how well the fault is projected onto the residual space, and (2) how high/low the threshold value is computed to be. To illustrate this important interaction between fault projection and threshold value, please refer to the two extreme situations presented below, both which represent an unsuccessful detection.

1. An unsuccessful detection caused by a relatively large threshold value (even though the fault projection onto the residual space is "good") as shown in Figure 10.

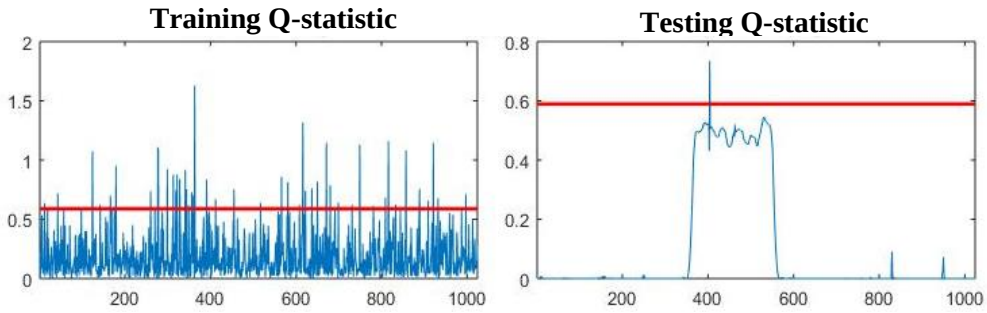

Figure 10: Unsuccessful detection due to high threshold.

2. An unsuccessful detection caused by a "bad" (i.e., small) fault projection onto the residual space as shown in Figure 11.

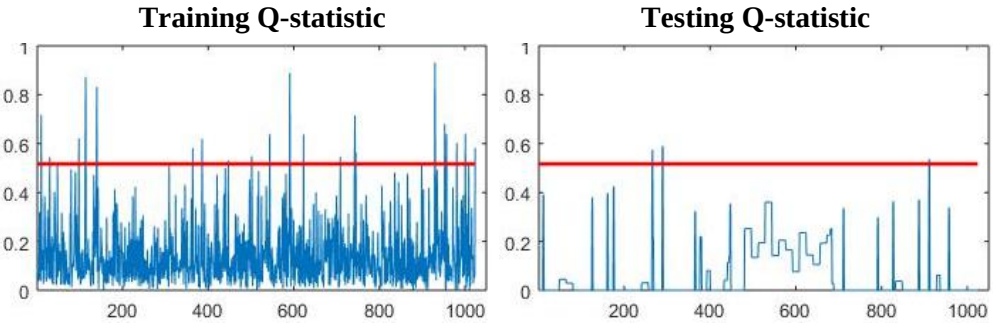

Figure 11: Unsuccessful detection due to poor fault projection.

It is important to note here, that, how well the data are projected onto the residual space is a direct consequence of the PCA model which is built from the *training data*. The extreme cases, i.e. a 0% detection rate, that results from poorly projected faults, allude to an issue of the data (or the model) *itself,* which does not concern the scope of this work.

However, sometimes the fault is “detectable” due to a good (or large) enough projection onto the residual space, but the conventional method will still not detect it. Figure 10 illustrates such a scenario. To further explore and identify those specific cases, please refer to Figure 12 that shows a plot of the residual fault projection versus the threshold value. The red crosses symbolize a DR less than 50% and the black crosses symbolize a DR greater than 50%.

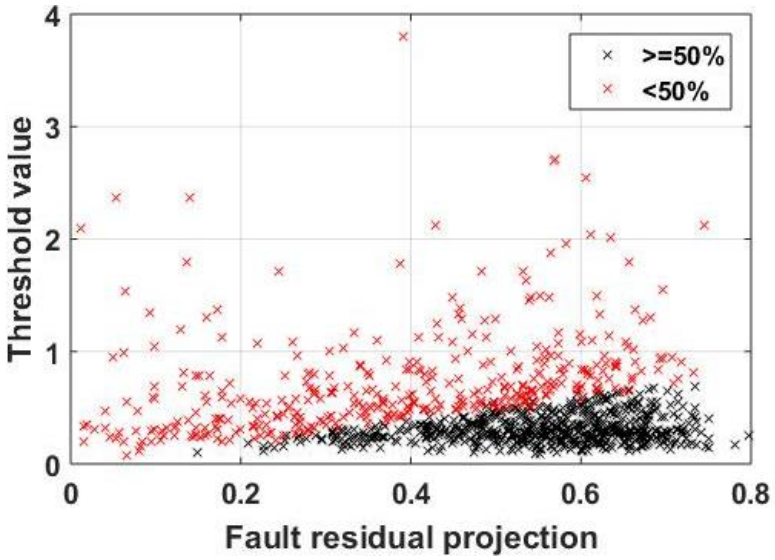

Figure 12: Analysis of the relationship between threshold value and fault projection for a successful detection.

The clear separation between the black and red marks in Figure 12 suggests that high threshold values are a key reason why the conventional method has a large count of unsuccessful detections. Figure 12 also accurately illustrates that detection is *always* bad for small fault projections on the residual space (specifically in the range 0 to 0.2). The

higher the fault projection, the more leeway MSPCA has with respect to the range of acceptable threshold values that give a high detection rate, as indicated by the gradually increasing black area.

Therefore, the conventional method performs most reliably for larger fault projections where the detection threshold can easily capture the fault. This work will tackle this issue by developing a more robust method that can successfully determine suitable thresholds for a wider range of fault projections. To do so, the developed technique will address the mismatch between the way the training and testing data are processed, specifically the selection rules which determines the wavelet coefficients that are selected for reconstruction. This will enable tighter detection thresholds that will lead to a higher DR. Furthermore, to maintain a low FAR, an additional soft-thresholding step will be used.

2.6. Enhanced MSPCA (EMSPCA) Algorithm

This section presents an enhanced MSPCA method that uses a different set of wavelet selection rules from those used in the conventional MSPCA method. The new way of processing wavelet coefficients will naturally yield a tighter and more adaptable threshold, which will improve the DR. It will also utilize soft-thresholding to reduce the FARs. The main steps in the EMPSCA algorithm are the same as the ones illustrated in Figure 7. First, the data is standardized to zero mean and unit variance. Then, wavelet transforms decompose the training and testing data into several scales. The training data is used to generate the PCA models and the detection thresholds to be utilized in detect significant features in the testing data at each scale. Afterwards, the detection criteria or the selection

rules will be implemented to select certain coefficients/scales for reconstruction, as described next.

2.6.1. Selection Rules in EMSPCA

The EMSPCA selection rules, unlike MSPCA, are not based on whether the scale is training or testing, rather, it is based on whether the scale is an *approximate* or a *detail*. The detail scales are the high frequency components and the approximate scale is the low frequency (slow changing) component of the decomposed process data. The new set of rules applied to both training and testing are:

1. Keep only the coefficients that violate the limits in the *detail* signals at each scale.
2. Always keep the entire *approximate* signal.

To further improve the detection results, soft-thresholding is applied on the detail signals of the testing data at each scale as will be described next.

2.6.2. Soft-Thresholding in EMSPCA

Soft-thresholding is sometimes called “wavelet shrinkage” because the values of the signals are being shrunk towards zero by subtracting the value of the threshold. In EMSPCA, it will be applied using the details signals as follows,

1. The Q statistic samples that don’t cross the detection threshold are set to zero.
2. The Q samples that cross the detection threshold are subtracted by the threshold value, and a new “soft-thresholded” Q statistic is generated.
3. The detection threshold is applied again on the soft-thresholded Q statistic and those samples that cross the limit are those selected for wavelet reconstruction.

Effectively, this is the same as using twice the threshold value. This step is critical for reducing the FAR in the testing data. The selected wavelet coefficients are reconstructed back to the time domain, where PCA fault detection is applied again.

2.6.3. Effect of Decomposition Depth and Fault Size on DR

A Monte Carlo simulation using 3000 realizations was used to evaluate the DR and FAR for MSPCA, EMSPCA, and EMSPCA-ST (with soft-thresholding). Figure 13 shows comparisons of the DR and FAR for the different techniques across nine wavelet decompositions depths using a fixed fault size of 1 sigma.

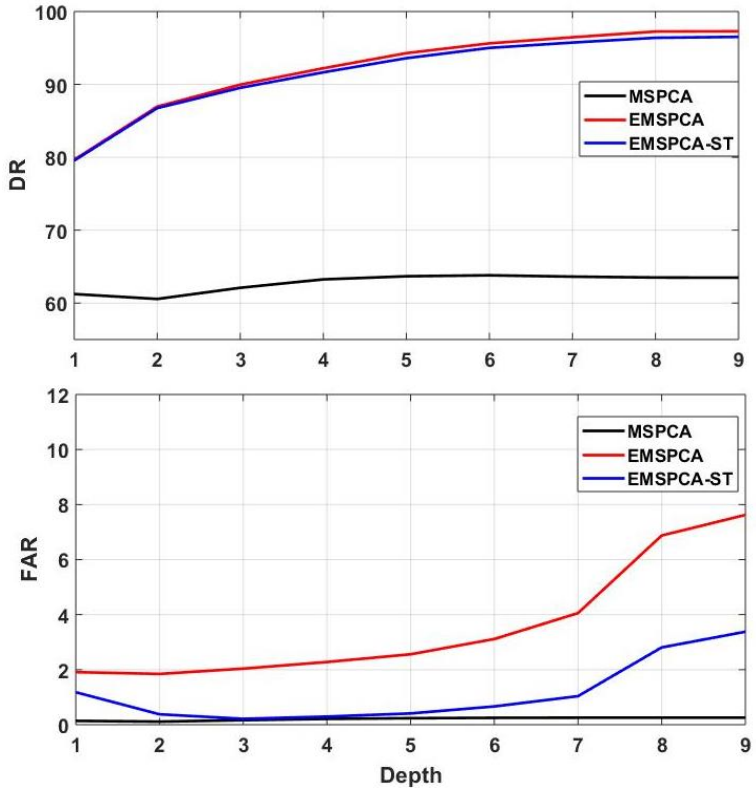

Figure 13: DR and FAR across 9 decomposition depths for MSPCA, EMSPCA, and EMSPCA-ST.

As illustrated in Figure 13, the EMSPCA method shows a large improvement in DR (about 25% higher than the conventional MSPCA) but suffers from a high FAR that reach up to 8% at large depths. This is due to the tight detection limits resulting from the new selection rules. However, when soft thresholding was used (EMSPCA-ST), the FAR was effectively reduced by more than two-fold while maintaining the high DR. The selection of the appropriate depth will therefore depend on the FAR tolerance; if FAR must be low (~ 0%), a depth of 5 can be used to achieve the highest DR for the required FAR.

A similar Monte Carlo simulation was used to evaluate the DR and FAR for MSPCA, EMSPCA, and EMSPCA-ST, but for varying fault sizes and a fixed depth of 4.

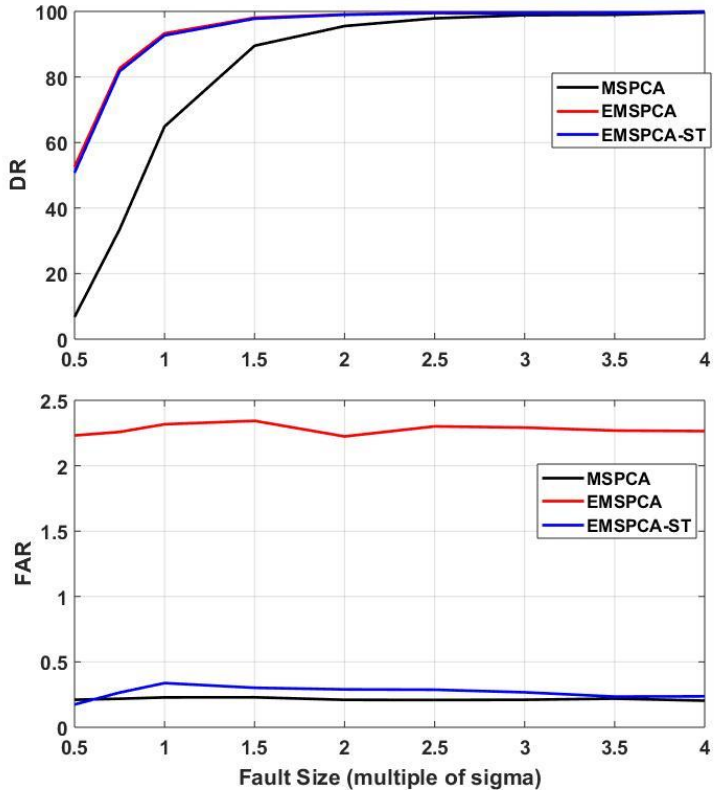

Figure 14: DR and FAR for different fault sizes for MSPCA, EMSPCA, and EMSPCA-ST.

Figure 14 shows that EMSPCA significantly improves detection rate for fault magnitudes less than 3 sigma. It also shows that implementing soft thresholding nicely fixes the issue of the high FAR. For brevity, EMSPCA will be used to refer to the technique that *uses* soft thresholding for the remainder of this paper. To further analyze the improvements achieved by the developed EMSPCA algorithm over the conventional MSPCA algorithm, please refer to Figure 15 and Figure 16 which highlight the robustness of the enhanced technique.

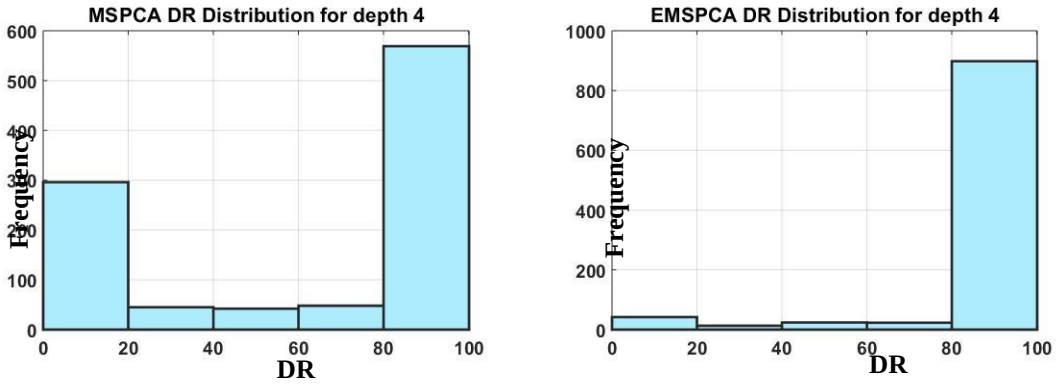

Figure 15: DR histogram distributions for MSPCA and EMSPCA for a depth of 4.

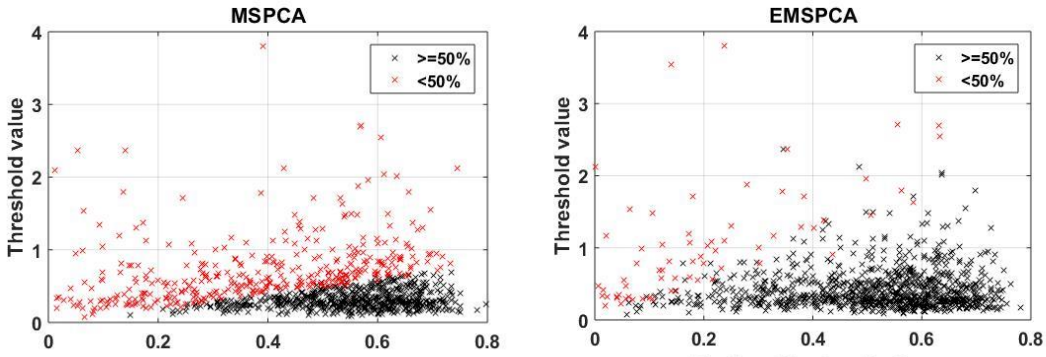

Figure 16: Analysis of the relationship between threshold value and fault projection for MSPCA and EMSPCA.

Figure 15 shows how the EMSPCA method significantly reduces the number of unsuccessful detections. Figure 16 shows that EMSPCA can determine more suitable threshold values (indicated by the increase in black markers), over a wider range of fault projections onto the residual space. This analysis shows that the developed EMSPCA method is more robust than the MSPCA for linear data sets with univariate faults.

2.6.4. Effect of Wavelet Decomposition Transform on DR

The decimated wavelet transform involves down-sampling while the undecimated wavelet transform does not. Thus, in the undecimated wavelet transform, the same number of samples is retained at every scale. The EMSPCA is implmeted using both wavelet transform methods: decimated and undecimated, and the DR and FAR are compared over all decomposition depths as shown in Figure 17.

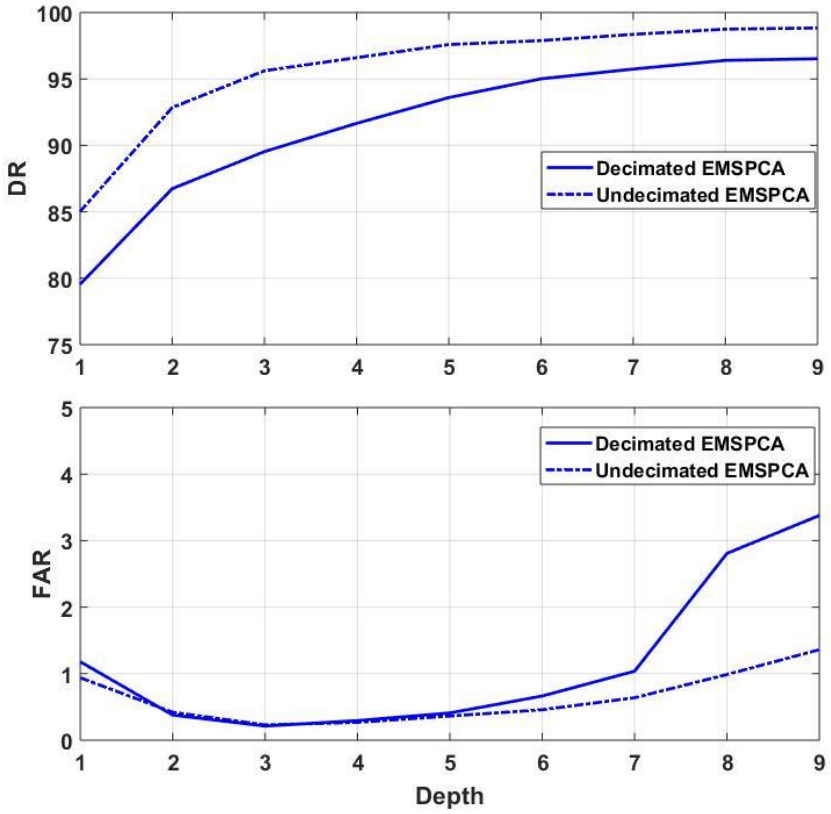

Figure 17: DR and FAR for decimated and undecimated EMSPCA.

Figure 17 shows that detection rate is improved by about 5% on average, and FAR is also improved (by being reduced) 1% on average when using the undecimated EMSPCA. This highlights the advantage of data redundancy of the undecimated wavelet transform for more effective fault detection.

Section 2 shows how EMSPCA significantly improves detection performance as it generates more accurate threshold values for the smaller range of fault projections. EMSPCA showed more reliable and accurate detection results. Furthermore, soft-thresholding the detail testing signals is a crucial step that significantly reduces the FAR. In the next section, EMSPCA will be extended to isolation to complete the FDI algorithm.

3. IMPROVING FAULT ISOLATION WITH EMSPCA

3.1. Introduction

Isolating the cause of a fault is just as important as detecting its presence for effective process monitoring. The previous section introduced EMSPCA to improve detection performance of conventional MSPCA. EMSPCA uses a different set of selection rules that can more accurately compute thresholds which result in better detection rates. The objective of this section is to extend EMSPCA to reconstructed-based isolation to improve isolation performance.

A multiscale framework has been utilized for isolation in 2001 and 2004 for a particular technique called complete decomposition (CD) also known as contribution plots [11][17]. The CD method is a popular PCA isolation technique that looks at individual variable contributions towards a detection index [14]. However, it suffers from smearing, which hinders correct isolation. Smearing occurs when variable contributions contaminate one another to the point where erroneous isolations occur [18]. Another isolation technique called the reconstruction-based (RB) method, which was established in 2008, is more robust towards smearing and can therefore outperform the conventional CD method in many cases [19]. Alcala et al. extensively analyzes the smearing effect in both the CD and the RB methods and concludes that the RB approach can guarantee fault isolation for large enough faults while the CD method cannot [20].

Therefore in this work, the reconstruction-based isolation approach will be integrated into EMSPCA algorithm for improved isolation performance. EMSPCA can provide

favorable detection rates, while the reconstruction isolation method is less susceptible to smearing. Additionally, this work will also compare the effect decimated and undecimated wavelet decompositions on the isolation rates.

The upcoming subsection 3.2 presents an introduction to PCA-based fault isolation. Subsection 3.3 will describe the proposed FDI algorithm based on EMSPCA. Subsection 3.4 will illustrate the performance of the developed FDI method using synthetic data. Section 4 and 5 will demonstrate the algorithm with real-data applications, namely, the TEP stripper and separator units and the pilot-plant lab data.

3.2. PCA Isolation

This section will only discuss the background related to PCA isolation. For an introduction to PCA and PCA detection, refer to Section 2.2. Fault isolation is the identification of the variable(s) causing a fault. This section will discuss the two main categories of PCA isolation methods: the general decomposition contributions (GD) (which is the general form of contribution plots), and the reconstruction-based methods [29]. However, there exists several fault isolation methods in literature (not within the scope of this work), and a review paper by Alcala et al. provides a good summary and an extensive analysis of the existing techniques [29].

Since detection precedes isolation, all the isolation contributions depend on the detection index used (Q, T^2 or φ). The isolation techniques will be discussed in their broad and general forms however they are implemented with respect to only the SPE or Q statistic in the Results of this work.

3.2.1. General Decomposition Method

The general decomposition contribution for a single variable i and a single measurement sample $\boldsymbol{x}$ is computed by the following equation [29],

$$GD_i^{index} = \boldsymbol{x^T M}^{1-\beta}\xi_i\xi_i^T\boldsymbol{M}^{\beta}\boldsymbol{x} \quad 0 \leq \beta \geq 1$$

where β is an arbitrary parameter between 0 and 1, ξ_i is called a direction vector with dimensions $m \times 1$, and it is ith column of the $m \times m$ identity matrix, and e subscript $index$ in GD_i^{index} can indicate Q when $\boldsymbol{M} = \widetilde{\boldsymbol{C}}$, T^2 when $\boldsymbol{M} = \widehat{\boldsymbol{P}}\widehat{\boldsymbol{\Lambda}}^{-1}\widehat{\boldsymbol{P}}^{\boldsymbol{T}}$, or φ when $\boldsymbol{M} = \frac{\widehat{\boldsymbol{P}}\widehat{\boldsymbol{\Lambda}}^{-1}\widehat{\boldsymbol{P}}^{\boldsymbol{T}}}{\tau^2} + \frac{\widetilde{\boldsymbol{C}}}{\delta^2}$ [29].

For $\beta = 0$ or $\beta = 1$, a method called the partial decomposition contribution (PD) is obtained. The PD index was developed for the T^2 statistic by Nomikos. It has the following general form [29],

$$PD_i^{index} = \boldsymbol{x^T M}\xi_i\xi_i^T\boldsymbol{x}.$$

This PD approach is not preferred for isolation because of the asymmetry in its form which does not guarantee a positive semidefinite matrix (even though $\boldsymbol{M}$ and $\xi_i\xi_i^T$ are both positive semidefinite). Consequently, counter-intuitive negative contribution values can be computed [29].

For $\beta = 1/2$, the formula reduces to a known method for fault diagnosis called *contribution plots*. It is also called complete decomposition contribution (CD), and the contribution of variable i has the following equation [29],

$$CD_i^{index} = \boldsymbol{x^T M}^{1/2}\xi_i\xi_i^T\boldsymbol{M}^{1/2}\boldsymbol{x} = \left(\xi_i^T\boldsymbol{M}^{\frac{1}{2}}\boldsymbol{x}\right)^{\boldsymbol{2}}.$$

The CD was originally developed for the Q statistic by Miller et al. [42], and was later implemented for the T^2 and for the combined index ϕ [43][29]. As the name suggests, the CD decomposes a particular index into its contributing components, such that the sum of all variable contributions yields the value of the detection statistic itself. The application of contribution plots for statistical process control (SPC) was introduced by MacGergor et al. (1996) for batch processes [44][45]. It has been successfully implemented in many industrial applications since then, and to name a few, Wang et al. (2004) identified faulty sensors in air handling units using SPE contributions [46], and Xiao et al. (2015) used both T^2 and SPE contributions to identify faults that occur in the rolling production of seamless tube process [47]. Due to its wide use and popularity, this work will consider the CD contributions or contribution plots as a basis and benchmark for comparison.

3.2.2. Reconstruction Based Method

The reconstruction methods is a category which involves PCA reconstruction (not to be confused with wavelet reconstruction). PCA reconstruction is the estimation of a variable using the PCA model and the other remaining variables (omitting the variable being estimated) under the objective of minimizing the error. Ideally, when the correct variable is reconstructed, the sample which used to contain a fault becomes fault free as illustrated by [6],

$$\boldsymbol{x}^{r_i} = \boldsymbol{x} - f\boldsymbol{\xi_i},$$

where, $\boldsymbol{x}^{r_i}$ represents the reconstructed sample, $\boldsymbol{x}$ is the testing data faulty sample, and $f\boldsymbol{\xi_i}$ is the fault component, represented as a direction ($\boldsymbol{\xi_i}$) and a fault magnitude (f). This interpretation works well in the case of univariate faults, however for multivariate faults,

one must reconsider the term $f\boldsymbol{\xi_i}$ which assumes that multiple variables are impacted by the same fault magnitude which is rarely the case [19]. Irrespective, the reconstruction-based isolation methods are centered on the idea that each variable reconstruction will result in new estimates of the T^2,Q or φ statistic [6]. The variable reconstruction which significantly lowers the detection statistic value (from its value before reconstruction) will have a higher fault isolation index, which signals the variable causing the fault.

Therefore, isolation accuracy is impacted by how well the PCA model can be used to reconstruct the values of each variable. Dunia et. al. introduced a parameter called the unreconstructed variance (URV) to measure the "goodness of reconstruction", and showed that a variable is unreconstructable when $c_{ii} = 1$ and $\tilde{\boldsymbol{\xi}}_{\boldsymbol{i}} = \mathbf{0}$, and poor reconstruction occurs when $c_{ii} \to 1$ and $\tilde{\boldsymbol{\xi}}_{\boldsymbol{i}} \to \mathbf{0}$ [48].

There are three similar and complimentary fault identification indices discussed: (1) reconstruction-based contributions (RB) , (2) sensor validity index (SVI) also called fault identification index (FII), and (3) angle based contribution (ABC) [29]. All three approaches are presented in their general forms which can accommodate any detection statistic with the choice of $\boldsymbol{M}$. The detection index for the reconstructed sample is computed by [29],

$$index(\boldsymbol{x}^{\boldsymbol{r_i}}) = \boldsymbol{x}^{r_i T}\boldsymbol{M}\boldsymbol{x}^{r_i} = \left\|\boldsymbol{M}^{\frac{\boldsymbol{1}}{\boldsymbol{2}}}\boldsymbol{x}^{r_i}\right\|^2 = \left\|\boldsymbol{M}^{\frac{\boldsymbol{1}}{\boldsymbol{2}}}(\boldsymbol{x} - f\boldsymbol{\xi_i})\right\|^2 = \left\|\boldsymbol{M}^{\frac{\boldsymbol{1}}{\boldsymbol{2}}}\boldsymbol{x}\right\|^2 - \left\|\boldsymbol{M}^{\frac{\boldsymbol{1}}{\boldsymbol{2}}}f\boldsymbol{\xi_i}\right\|^2,$$

which simplifies to,

$$index(\boldsymbol{x}^{\boldsymbol{r_i}}) = index(\boldsymbol{x}) - \left\|\boldsymbol{M}^{\frac{\boldsymbol{1}}{\boldsymbol{2}}}f\boldsymbol{\xi_i}\right\|^2$$

The term $\left\|\boldsymbol{M}^{\frac{1}{2}} f \boldsymbol{\xi}_i\right\|^2$ represents the reconstructed-based contribution (RB_i^{index}) for a variable i where the $index$ is based on a detection statistic used. An isolation index can be based on the Q, T^2 and φ, where $\boldsymbol{M}$ must equal $\widetilde{\boldsymbol{C}}$, $\widehat{\boldsymbol{P}}\widehat{\boldsymbol{\Lambda}}^{-1}\widehat{\boldsymbol{P}}^{\boldsymbol{T}}$, or $\frac{\widehat{\boldsymbol{P}}\widehat{\boldsymbol{\Lambda}}^{-1}\widehat{\boldsymbol{P}}^{\boldsymbol{T}}}{\tau^2} + \frac{\widetilde{\boldsymbol{C}}}{\delta^2}$. The RB contribution was established by Alcala et al. (2009) for all detection indices (T^2,Q and φ) [49].

Rearranging the above equation, we obtain,

$$RB_i^{index} = index(\boldsymbol{x}) - index(\boldsymbol{x}^{\boldsymbol{r}_i}),$$

where the RB_i^{index} represents the difference between the detection statistic before and after reconstruction. Dividing the above equation by $index(\boldsymbol{x})$ to obtain [29],

$$\frac{RB_i^{index}}{index(\boldsymbol{x})} = 1 - \frac{index(\boldsymbol{x}^{\boldsymbol{r}_i})}{index(\boldsymbol{x})}$$

where the term $\frac{RB_i^{index}}{index(\boldsymbol{x})}$ represents the angle-based contribution (ABC) and $\frac{index(\boldsymbol{x}^{\boldsymbol{r}_i})}{index(\boldsymbol{x})}$ represents the sensor validity index (SVI) or the fault isolation index (FII). Furthermore, both these indices are complimentary ($ABC = 1 - SVI$) [28]. The sensor validity index (SVI), was initially developed by Dunia et al. in 1996 for the Q detection statistic [48]. In 1998 it was termed the fault identification index (FII) for more general faults (not just sensor faults) [6]. ABC is a scaled version of the RB, initially used by Raich et al. in 1996 for both the Q and T^2 statistics [50].

This work will use the reconstruction based (RB) contribution because of the statistical simplicity that comes with its definition as a difference between detection indices, rather than the ratios [51]. Since the detection is restricted to the Q statistic only,

the RB contribution equation, written in terms of, the sample vector $\boldsymbol{x}$, residual model $\widetilde{\boldsymbol{C}}$, and the fault direction ξ_i^T, is as follows [20],

$$RB_i^Q = \frac{\left(\xi_i^T \widetilde{\boldsymbol{C}} \boldsymbol{x}\right)^2}{\tilde{c}_{ii}}.$$

3.2.3. Smearing Effect

The CD and RB fault isolation indices suffer from a phenomena called the smearing effect. The smearing effect is when a fault in variable j can impact the fault isolation indices of the other variables, and when the impact is sufficiently large, such that the contribution of a non-faulty variable i is greater than the contribution of the faulty variable j, it will lead to misdiagnosis [20]. The CD and RB equations for a system of 4 variables, is illustrated below to highlight the naturally occurring phenomena. As can be seen, the index for variable 1 is computed from the values of the other 4 variables. The severity of smearing is determined by the relative magnitudes of the coefficients.

$$CD_1^{SPE} = (\widetilde{\boldsymbol{c_1}}\boldsymbol{x})^{\boldsymbol{2}} = \left([\tilde{c}_{11} \quad \tilde{c}_{12} \quad \tilde{c}_{13} \quad \tilde{c}_{14}] \begin{bmatrix} x_1 \\ x_2 \\ x_3 \\ x_4 \end{bmatrix} \right)^2$$

$$RB_1^{SPE} = \frac{(\widetilde{\boldsymbol{c_1}}\,\boldsymbol{x})^2}{\tilde{c}_{11}} = \left([\tilde{c}_{11} \quad \tilde{c}_{12} \quad \tilde{c}_{13} \quad \tilde{c}_{14}] \begin{bmatrix} x_1 \\ x_2 \\ x_3 \\ x_4 \end{bmatrix} \right)^2 * \frac{1}{\tilde{c}_{11}}$$

Smearing will always be an issue because PCA involves projecting data into dimensions of lower rank, introducing interdependencies between variables, which unavoidably causes smearing [52]. Yoon and MacGregor apply contribution plots to a CSTR reactor model where the smearing effect led to a misdiagnosis [18]. A work by

Alcala et al. in 2011 examined smearing in both the contribution plot (or CD) and the reconstruction based contribution (RB) methods, and concluded, that RB can guarantee fault diagnosis for large enough faults (despite smearing effects) while the traditional contribution plot cannot [20]. This suggests that RB isolation approach is less prone to smearing failure than the CD approach, which motivates the idea of developing a multiscale fault isolation algorithm based on the RB approach.

3.2.4. Control Limits for Isolation

Even when there is no fault, the contributions of each variable towards a detection index varies because of smearing. Therefore, a single control limit cannot be used to identify whether or not a variable is faulty [53]. Previous works have proposed the following limits, specific to an individual variable, for the CD and RB indices computed from fault-free data [28],

$$CD\gamma_i^2 = \xi_i^T \boldsymbol{S}\widetilde{\boldsymbol{C}}\xi_i \chi_\alpha^2(1)$$

$$RB\gamma_i^2 = \frac{\xi_i^T \widetilde{\boldsymbol{C}}\boldsymbol{S}\widetilde{\boldsymbol{C}}\xi_i}{\xi_i^T \widetilde{\boldsymbol{C}}\xi_i} \chi_\alpha^2(1)$$

Due to the effects of smearing, it is safer to base fault diagnosis on the relative magnitudes of the contributions. Therefore, for unidimensional faults, the faulty variable is identified by the largest fault isolation contribution, and several works have used this criteria [19] [11] [54] [55].

As indicated earlier, this work aims at developing a full FDI algorithm which integrates the EMSPCA fault detection algorithm with a new multiscale reconstruction

based fault isolation approach. The developed enhanced multiscale PCA fault detection and isolation (EMSPCA FDI) algorithm is described next.

3.3. EMSPCA Isolation Algorithm

The EMSPCA fault detection algorithm is a modified version of the conventional MSPCA algorithm. For a description of the MSPCA algorithm refer to section 2.4. EMSPCA was developed to improve the accuracy of fault detection; it provides higher detection rates than the conventional method due to the modified set of rules or criteria for selecting the significant wavelet coefficients used in its implementation.

As in MSPCA, EMSPCA starts with training data to build the PCA models and the set of normal-operating limits to be used for the testing data as follows:

For the Training Data:

1. Standardize the data to zero mean and unit variance.
2. Decompose the data at multiple scales using wavelet decomposition (DWT or UWT).
3. Determine and store the PCA models and detection thresholds for every scale.
4. Select the detail and approximate coefficients using the detection criteria, which involves computing the Q statistic for the *details* and selecting only the samples which cross the Q-threshold, and selecting *all* the *approximate* coefficients with no consideration towards the Q statistic.
5. Reconstruct the selected coefficients back to the time domain.
6. Determine the PCA model and detection threshold for the time domain reconstructed signal.

The key difference between EMSPCA and MSPCA is in step 4 which revolves around the detection criteria that is used to determine which coefficients are reconstructed back to the time domain. Unlike EMSPCA, which applies *different* selection rules to the detail

and approximate scales, the conventional MSPCA applies the *same* rule on both the detail and approximate scales. MSPCA states that if at least one sample crosses the threshold in the training scales, retain the entire scale for reconstruction. While EMSPCA, always keeps the approximate scale and only retains coefficients that cross the threshold of the detail scales. The testing data algorithm is illustrated in Figure 18, and described by steps afterwards.

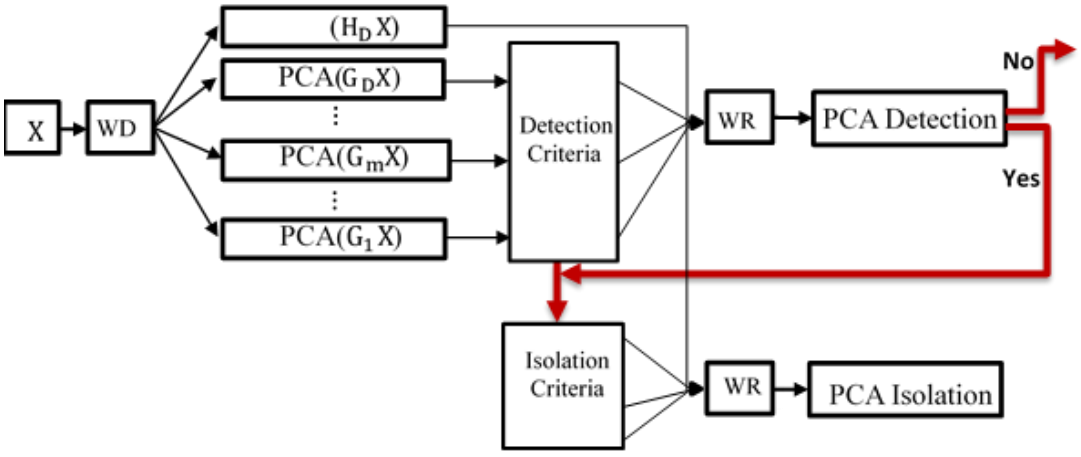

Figure 18: Complete EMSPCA-detection and isolation algorithm diagram.

For the Testing Data:

1. Preprocess the data; standardize with the mean and variance of training data.
2. Decompose the data at multiple scales using wavelet decomposition WD (DWT or UWT).
3. Use the PCA models to compute the detection statistic for the detail signals.
4. Apply soft thresholding on the detection statistic of the details. Soft thresholding involves shrinking the Q statistic towards zero by the value of the threshold itself,

which effectively reduces the amount of samples that cross the detection Q threshold.

5. Apply the detection criteria to determine the selected coefficient for reconstruction. The detection criteria is the same one that was described previously in step 4 of the Training Data Algorithm.
6. Reconstruct the selected coefficients back to the time domain (WR).
7. Carry out fault detection using the reconstructed time domain data.

MSPCA isolation occurs only when a fault is detected (i.e., the detection limit is crossed). So in the **event of a fault** steps 8 through 11 are carried out,

8. Compute the isolation indices at every scale for the selected coefficients from the detection criteria.
9. Select the coefficient corresponding to the faulty variable (i.e., the variable with the largest isolation contribution).
10. Reconstruct the selected coefficients to the time domain.
11. Carry out RB fault isolation using the reconstructed time domain data.

The key difference between EMSPCA and MSPCA for the testing data algorithm lies in step 4 and 5. Soft thresholding (step 4) is a new addition to the algorithm that was made to reduce false alarms. Furthermore, the EMSPCA detection criteria excludes the approximate signal from being subjected to detection thresholding, while in MSPCA, the approximate signal is not.

The novelty of this algorithm lies in its extension to isolation. As can be seen, both detection and isolation criteria's are used for selecting the significant detail coefficients; the detection criteria helps select the significant features for fault detection and the isolation criteria further removes features that would hinder fault isolation. The process of

selecting the significant coefficients from every detailed scale is methodically illustrated in Figure 19.

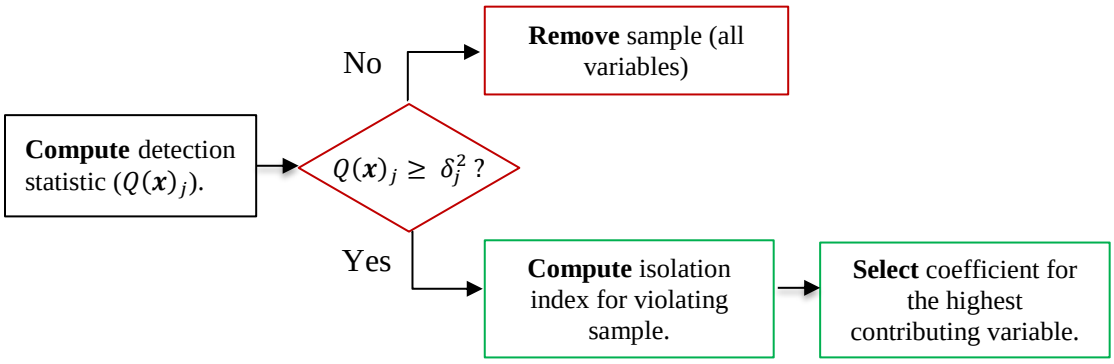

Figure 19: Detection and isolation criteria for selecting significant coefficients.

In the upcoming section, the EMSPCA algorithm, will be implemented with synthetic data to evaluate its isolation performance. The performance of the different isolation techniques RB and CD will be compared and the improvements made to traditional PCA isolation will be demonstrated.

3.4. Illustrative Example: Synthetic Data

This section will use a synthetic model to evaluate the fault isolation performance of the proposed EMSPCA FDI algorithm. The fault detection performance has previously been studied in section 2.6. The fault isolation performance is evaluated by the fault isolation rate (FIR), which is defined as, $FIR = \frac{number\ of\ correctly\ identified\ faulty\ variables}{number\ of\ detected\ faulty\ samples} * 100$ [56].

The process model used in this example has a total of 6 dependent variables that are a function of 3 independent variables as shown below,

$$\begin{bmatrix} x_1 \\ x_2 \\ x_3 \\ x_4 \\ x_5 \\ x_6 \end{bmatrix} = [M] \begin{bmatrix} t_1 \\ t_2 \\ t_3 \end{bmatrix} + noise$$

where $t_1 \sim 1N(0,1)$, $t_2 \sim 0.8N(0,1)$, $t_3 \sim 0.6N(0,1)$, $noise \sim 0.2N(0,1)$, and M is a 6×3 matrix and its elements are randomly generated from a $N(0.2, 1)$ distribution. In all cases studied in this Section, a Monte Carlo simulation using 3000 realizations is performed to achieve statistical meaningful results. Furthermore, to eliminate the effect of the choice of faulty variable and fault location, a fault is introduced to a random variable and at a random location in each realization. Two data sets are generated; a training data set (fault free) and a testing data set with a bias fault that spans 200 samples.

3.4.1. Effect of Fault Size on FIR

The section examines how fault size impacts the fault isolation rate (FIR) using the synthetic model. The performances of the multiscale isolation methods, EMSPCA-RB and EMSCPA-CD will be assessed and compared to their traditional PCA counterparts, PCA-RB and PCA-CD. A Monte Carlo simulation of 3000 realizations is utilized to obtain meaningful conclusions, and the results are shown in Figure 20 for all aforementioned isolation methods. In all multiscale simulations, a decomposition depth of 4 is used because it was found to provide good detection rates in Section 2.6.

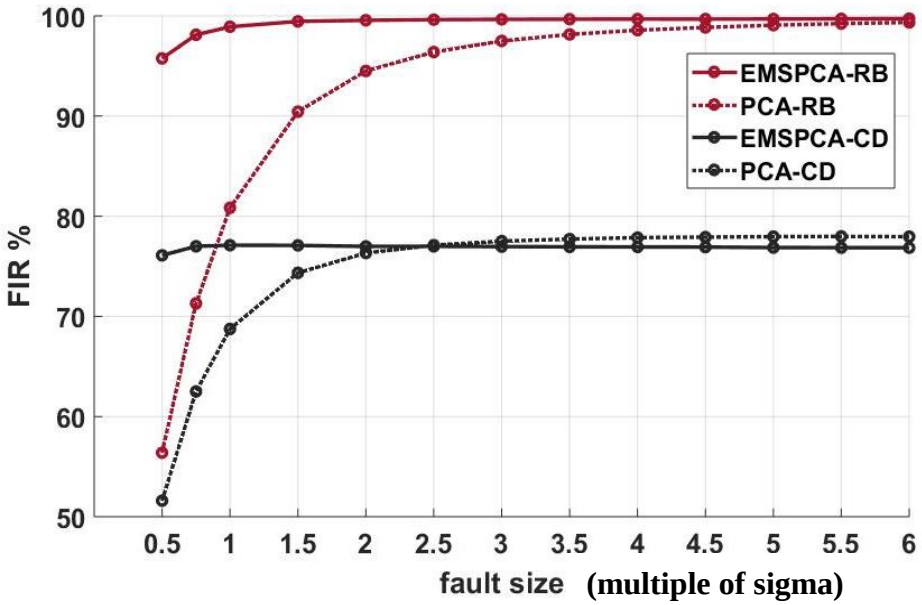

Figure 20: Effect of fault size on RB and CD FIR for PCA and EMSPCA.

It has been reported by several researchers that the PCA-RB isolation method outperforms the PCA-CD isolation method, which is clearly demonstrated by the dotted lines in Figure 6 [57]. This is because the PCA-RB method is less impacted by smearing [52]. For large-enough faults (5.5 sigma) the PCA-RB isolation rate reaches almost 100%, while the PCA-CD isolation rate plateaus at below 80%. This result is in agreement with Alcala et al. work which states that for a large enough fault, the RB method can guarantee correct isolation while CD cannot [28].

Figure 20 also shows that there is a significant improvement in the fault isolation rates obtained by the EMSPCA techniques compared to their traditional PCA counterparts, specifically for smaller fault sizes. This is due to the ability of multiscale representation to separate deterministic and stochastic features (noise) in the data and thus reducing the

effect of noise on fault isolation. It is important to note that noise can also smear into variables' contributions used to isolate fault, and hence can affect the accuracy of isolation. That's why the advantages of the multiscale techniques are more notable for small faults, where the relative contribution of noise is higher. Furthermore, the EMSPCA-RB isolation method outperforms all other methods; even for a small fault of 0.5 sigma, it is able to correctly isolate it 93% of the time, compared to the traditional PCA method at 55% and the MSPCA-CD method at 78%.

As indicated earlier, the fault isolation results presented earlier were generated using a fixed decomposition depth of 4. In the next section, the effect of different decomposition depths on the isolation rate will be assessed.

3.4.2. Effect of Decomposition Depth on FIR

The EMSPCA algorithm can be implemented with any decomposition depth between 1 and $\log_2$ (number of samples). This section examines the effect of decomposition depth on the fault isolation rate. The results were generated using the synthetic model with a fixed fault size of 1 sigma and a Monto Carlo simulation of 3000 runs. Furthermore, the effect of decimation, i.e., utilizing the DWT or UWT in each isolation scheme, will also be observed. Figure 21 presents the isolation performance for the decimated and undecimated EMSPCA algorithm for the RB and CD based techniques.

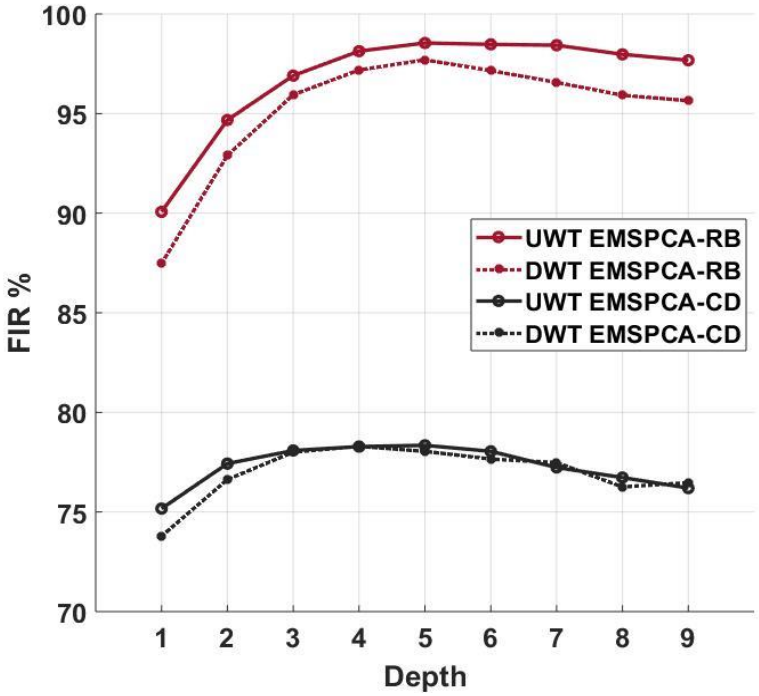

Figure 21: FIR across 9 decomposition depths at a fixed fault of 1 sigma for decimated and undecimated wavelet transforms.

As anticipated from the previous discussion, the RB based isolation outperforms the CD based methods due to higher robustness to smearing. Figure 21 indicates this information regardless of the decomposition depth, RB is about 15-20% more accurate in isoalting the fault. Secondly, all assessed fault isolation methods (including the decimated and undecimated schemes) show a similar graphical pattern: the FIR increases to a peak and then decreases. Starting at depth 1, increasing the depth improves the FIR because valuable feature-extraction is obtained by representing the data at multiple scales. However, once the signal reaches the optimal FIR, increasing the depth will reduces the

FIR because decomposing the data to very coarse scales start eliminating important features in the data.

Furthermore, the undecimated EMSPCA-RB isolation rate in Figure 21 consistently outperforms the decimated EMSPCA-RB isolation rate by a margin of about 2%. This is because more data is available at each in the undecimated approach (compared to the smaller data sizes at coarser scales in the decimated approach), which provides more data to construct more accurate models and more accurate statistics. However, the impact of decimation on the EMSPCA-CD approach is less evident. This suggests that CD methods are not impacted by the mode of decomposition as much as they are by the smearing phenomena.

4. TENNESSEE EASTMAN PROCESS APPLICATION

The Tennessee Eastman Process (TEP) is a well-known benchmark process used by the research community to evaluate process control and monitoring methods with simulated process faults [13].

4.1. Description of Process

The TEP contains 5 major units: a reactor, condenser, stripper, separator and a compressor. There are 4 reactants (A, C, D, and E), 1 inert (B), 2 desired products (G, H), and a byproduct (F) [58]. The process flow diagram is shown in Figure 22, modified from [58]. Pure A, D and E are mixed with the recycle stream that is fed into the reactor. The products leaving the reactor are cooled with a condenser and enter a vapor liquid separator. The overhead products of the separator are recycled back to the reactor, while the bottoms are further purified in the stripper. There is a total of 4 different control strategies based on a single-input single-output PID controllers that have been developed for the TEP [59].

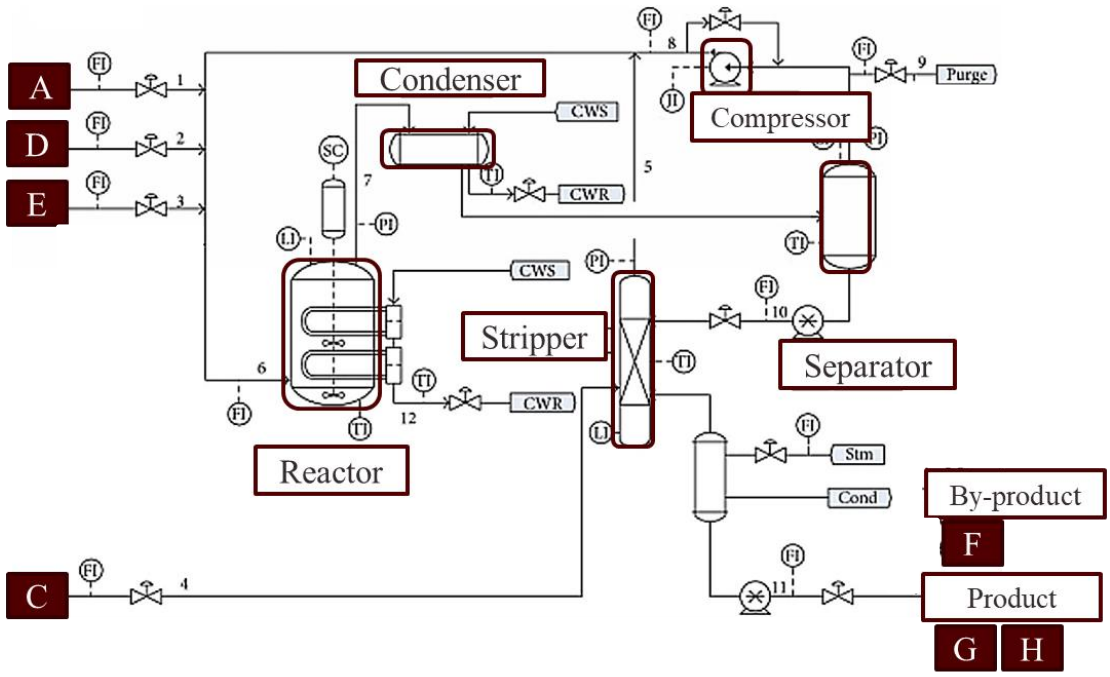

Figure 22: TEP process flow diagram (adapted [58]).

There is a total of 41 measured variables and 12 manipulated variables, all of which are tabulated in Table 2 [58].

Table 2: TEP measured and manipulated variables [58]**.**

#	***Measured Variable***	*#*	***Measured Variable***	*#*	***Manipulated Variable***
1	A Feed (stream 1)	22	Sep Cooling Water Outlet Temperature	1	D Feed (stream 2)
2	B Feed (stream 2)	23	Composition A (stream 6)	2	E Feed (stream 3)
3	E Feed (stream 3)	24	Composition B (stream 6)	3	A Feed (stream 1)
4	Total Feed (stream 4)	25	Composition C (stream 6)	4	Total Feed (stream 4)
5	Recycle Flow (stream 8)	26	Composition D (stream 6)	5	Compressor Recycle Valve
6	Reactor Feed Rate	27	Composition E (stream 6)	6	Purge Valve
7	Reactor Pressure	28	Composition F (stream 6)	7	Sep Pot Liquid Flow (st 10)
8	Reactor Level	29	Composition A (stream 9)	8	Stripper Liquid Product Flow (st 11)
9	Reactor Temperature	30	Composition B (stream 9)	9	Stripper Steam Valve
10	Purge Rate (stream 9)	31	Composition C (stream 9)	10	Reactor Cooling W Flow
11	Product Sep Temp	32	Composition D (stream 9)	11	Condenser Cooling W Flow
12	Product Sep Level	33	Composition E (stream 9)		
13	Product Sep Pressure	34	Composition F (stream 9)		
14	Product Sep Underflow	35	Composition G (stream 9)		
15	Stripper Level	36	Composition H (stream 9)		
16	Stripper Pressure	37	Composition D (stream 11)		
17	Stripper Underflow	38	Composition E (stream 11)		
18	Stripper Temperature	39	Composition F (stream 11)		
19	Stripper Steam Flow	40	Composition G (stream 11)		
20	Compressor Work	41	Composition H (stream 11)		
21	Reactor Cooling Water Outlet Temp				

The TEP data was acquired from the online open source simulator [60]. For the purpose of this work, individual units in the TEP will be monitored independently because correlation among variables is stronger with fewer numbers and when the variables are

within a close proximity of each other. The two units monitored in this section are the stripper and the separator units.

4.2. FDI Performance I: Separator Unit

The function of the separator in the TEP is to remove the vapor, which contains unreacted raw material, from the liquid, which contains most of the TEP products. A labeled diagram of the monitored variables of the separator unit is shown in Figure 23 alongside Table 3 with the variable descriptions.

Table 3: TEP separator variables.

#	***Separator Variables***
1	Purge Rate (stream 9)
2	Product Sep Temp
3	Product Sep Level
4	Product Sep Pressure
5	Compressor Recycle Valve
6	Purge Valve

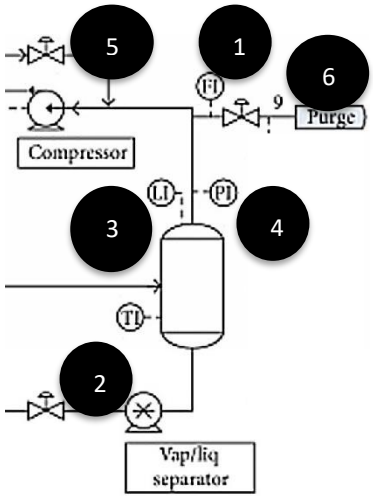

Figure 23: TEP separator unit.

For this study, a confidence level of 98% was used for thresholding of the detail signals, and a 95% confidence level was used for detection in the reconstructed time domain signal. A decomposition depth of 4 and a CPV of 90% are used. A step fault of size 1.4 sigma is introduced to variable 1 (the purge flowrate) from sample 200 to 500. Figure 24 presents the plots for the training and testing data sets.

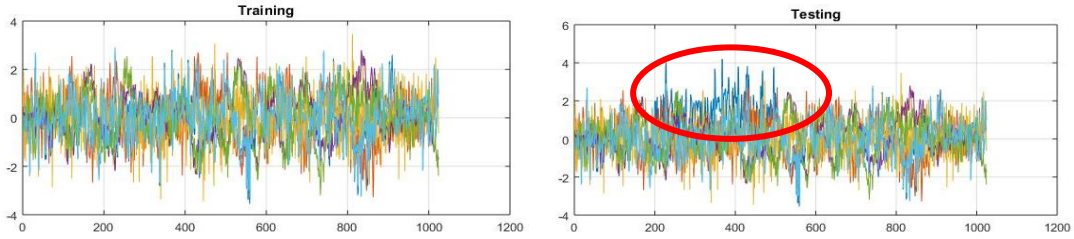

Figure 24: Training and testing data for TEP separator.

4.2.1. Fault Detection Results

The fault detection performance is evaluated with 5 different methods: traditional PCA, decimated MSPCA, undecimated MSPCA, decimated EMSPCA, and undecimated EMSPCA. Table 4 presents the FAR, DR, and the number of PCs used to build the model for this example.

Table 4: Separator fault detection results.

	Training Data	**Testing Data**	
Case	**# of PCs**	DR	FAR
PCA	4	55.482	6.3624
MSPCA -dec	4	39.203	2.213
MSPCA -und	4	21.595	1.1065
EMSPCA -dec	3	95.681	3.3195
EMSPCA -und	3	100	2.4896

Table 4 shows the superior detection performance of the EMSPCA algorithm with detection rates greater than 95%. It also shows the case where the conventional MSPCA

algorithm performs worse than the traditional PCA method. For a visual representation of the tabulated results, refer to Figure 25.

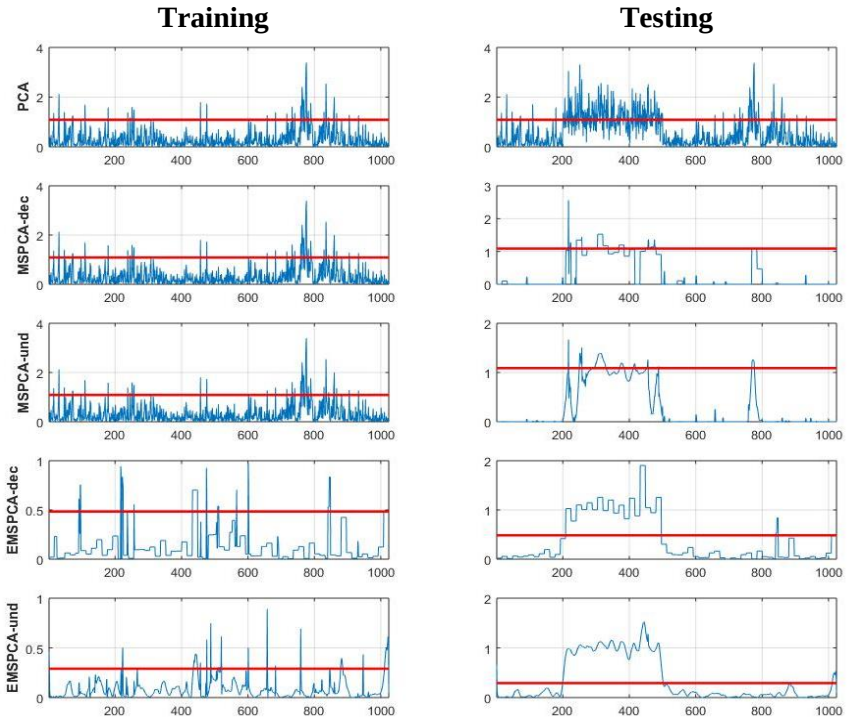

Figure 25: TEP separator testing and training Q-statistic.

As can be seen in Figure 25, MSPCA fails to correctly capture the fault projection with the computed threshold, while the EMPSCA method could. Therefore, this example illustrates the advantages of the new thresholding/selection rules of EMSPCA, which produce more accurate detection thresholds and a better overall performance.

Furthermore, the fault abruptly falls below the threshold in the testing data of the MSPCA method. This is a result of the final *approximate signal* being subjected to PCA

thresholding by the MSPCA selection rules. When the fault is relatively small, some or many samples in the approximate signal will not be selected for reconstruction, which affects the quality of the detection performance as exemplified by Figure 25 and the results in Table 4. However, in EMPCA the approximate signal is not subjected to any criteria and it is always retained, thus, the abrupt dips in the faulty region are not observed.

Additionally, the undecimated EMPCA algorithm has a slightly better detection performance than that of the decimated EMSPCA. This is due to the desired redundancy in the MS coefficients, which enable a more accurate representation of the changes that occur in a signal.

4.2.2. Fault Isolation Results

Two isolation techniques, the RB and CD method, are tested and compared for the EMSPCA and the traditional PCA methods. Table 5 summarizes the results.

Table 5: FIR results for TEP separator.

	FIR %	
Method	**RB**	**CD**
PCA	47.305	37.725
EMSPCA (dec)	61.111	33.333
EMSPCA (und)	89.226	82.155

The undecimated EMSPCA method has an RB and CD isolation rate that is roughly 43% and 45% better than the traditional PCA RB and CD isolation rates. Furthermore, the RB isolation method is consistently better than the CD method because it is more robust towards smearing. To illustrate the smearing effect visually, a point was

plotted to mark the “identified” faulty variable (y-axis) at every sample (x-axis) in Figure X. The faulty variable that was correctly detected and isolated is in black while the other points are in blue. The faulty region is highlighted in purple.

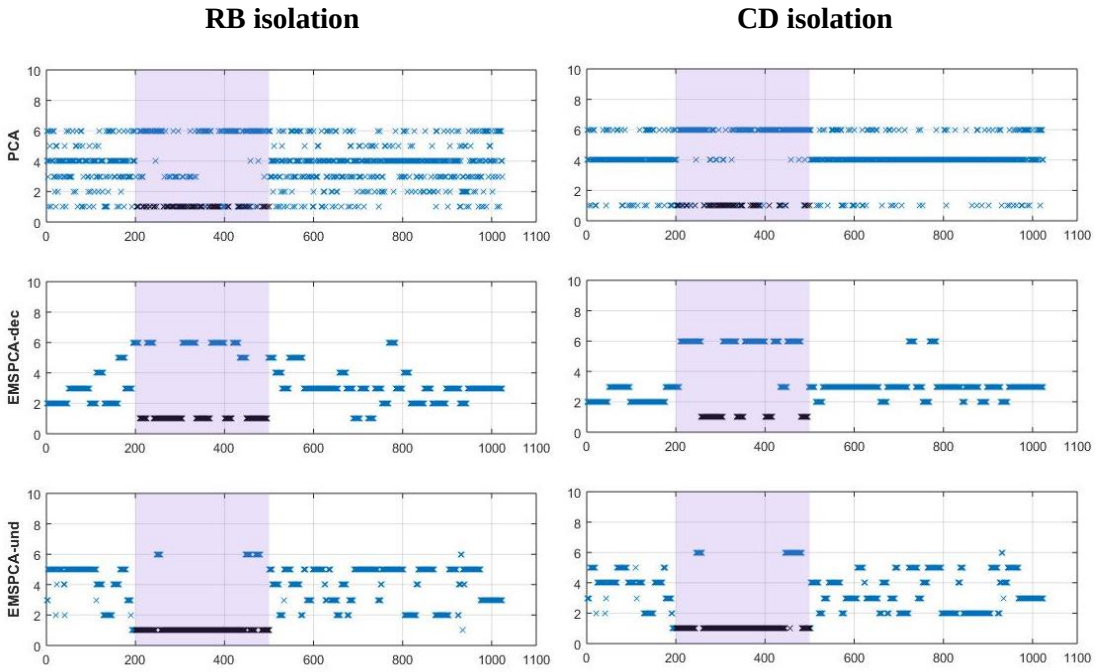

Figure 26: TEP separator RB and CD isolation results.

From Figure 26, one can see how smearing of the fault is a major issue for the PCA method using both RB and CD techniques and less so for the EMSPA methods. The smearing is mostly reduce by the undecimated EMSPCA method.

4.3. FDI Performance II: Stripper Unit

The function of the stripper is to further purify the liquid coming from the separator. A labeled diagram of the monitored variables of the stripper unit is shown in Figure 27.

Table 6: TEP stripper variables.

#	***Stripper Variables***
1	Stripper Level
2	Stripper Pressure
3	Stripper Underflow
4	Stripper Temperature
5	Stripper Steam Flow
6	Stripper Steam Valve

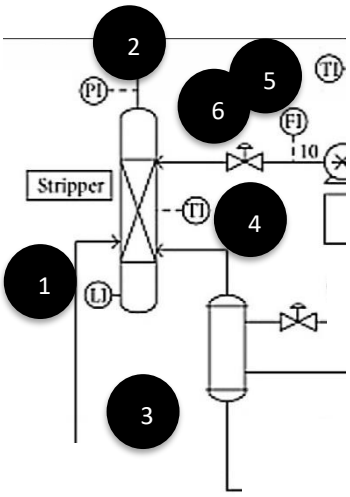

Figure 27: TEP stripper unit.

The same parameters (decomposition depth of 4 and a CPV of 90%) and confidence levels (98% and 95%) of the previous test were also utilized for this example. However for this study, a lower step fault of size 0.8 sigma is introduced to variable 5 (the stripper steam flowrate) from samples 200 to 500. Figure 28 presents the plots for the training and testing data sets.

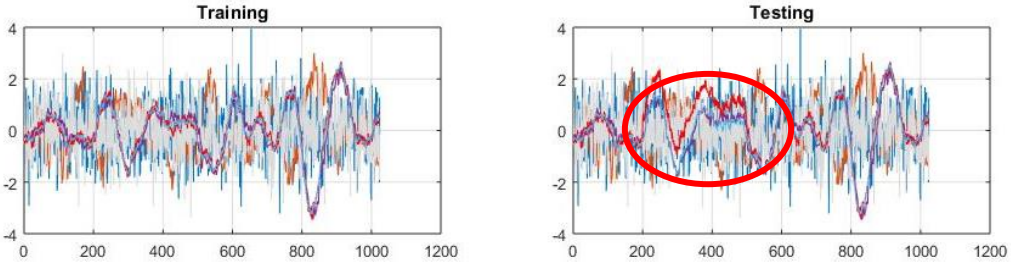

Figure 28: Training and testing data for TEP stripper unit.

4.3.1. Fault Detection Results

The fault detection performance is evaluated with traditional PCA, decimated MSPCA, undecimated MSPCA, decimated EMSPCA, and undecimated EMSPCA. Table 7 presents the FAR, DR, and the number of PCs used to build the model in this simulation.

Table 7: TEP stripper fault detection results.

	Training Data	**Testing Data**	
Case	**# of PCs**	DR %	FAR %
PCA	4	98.007	6.9156
MSPCA -dec	4	58.472	0.13831
MSPCA -und	4	82.392	0
EMSPCA -dec	2	71.761	2.213
EMSPCA -und	2	98.671	1.6598

As can be seen from Table 7, EMSPCA consistently outperforms MSPCA. For the decimated case, EMSPCA performs about 13% better in detection rate, and for the undecimated case, EMSPCA performs about 16% better in detection rate. The traditional

PCA has a DR of 98%, which is about same as the DR for the undecimated EMSPCA, however, PCA suffers from a relatively high FAR of about 7% when compared to 1.7% of EMSPCA. This indicates the de-noising advantage brought about by multiscale analysis. The Q statistics for the training and testing data are illustrated in Figure 29.

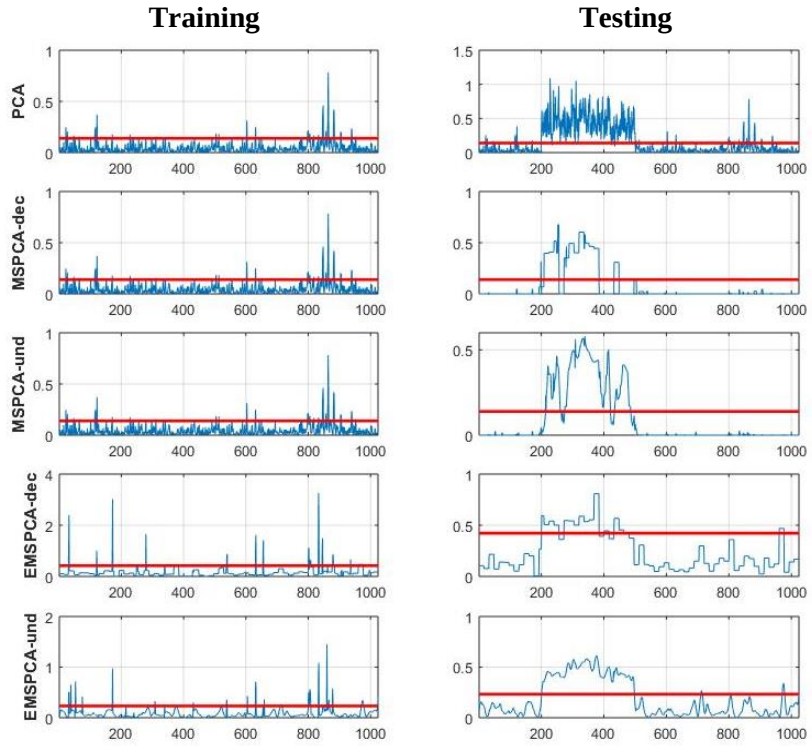

Figure 29: TEP stripper testing and training Q-statistic.

As can be seen from Figure 29, the fault appears clearly in the Q statistic for all the methods, however, the decimated and undecimated MSPCA testing data plots have regions where the fault radically falls below the threshold. This trend was also noticed in the previous application and is due to the thresholding of the approximate signal.

Furthermore, applying the undecimated wavelet transform improves the performance of MSPCA and EMSPCA.

4.3.2. Fault Isolation Results

The RB and CD isolation techniques are tested and compared for the traditional PCA and EMSPCA methods. The results are summarized in Table 8 and illustrated in Figure 30.

Table 8: FIR results for TEP stripper.

	FIR %	
Method	**RB**	**CD**
PCA	94.595	97.97
EMSPCA (dec)	100	85.185
EMSPCA (und)	100	100

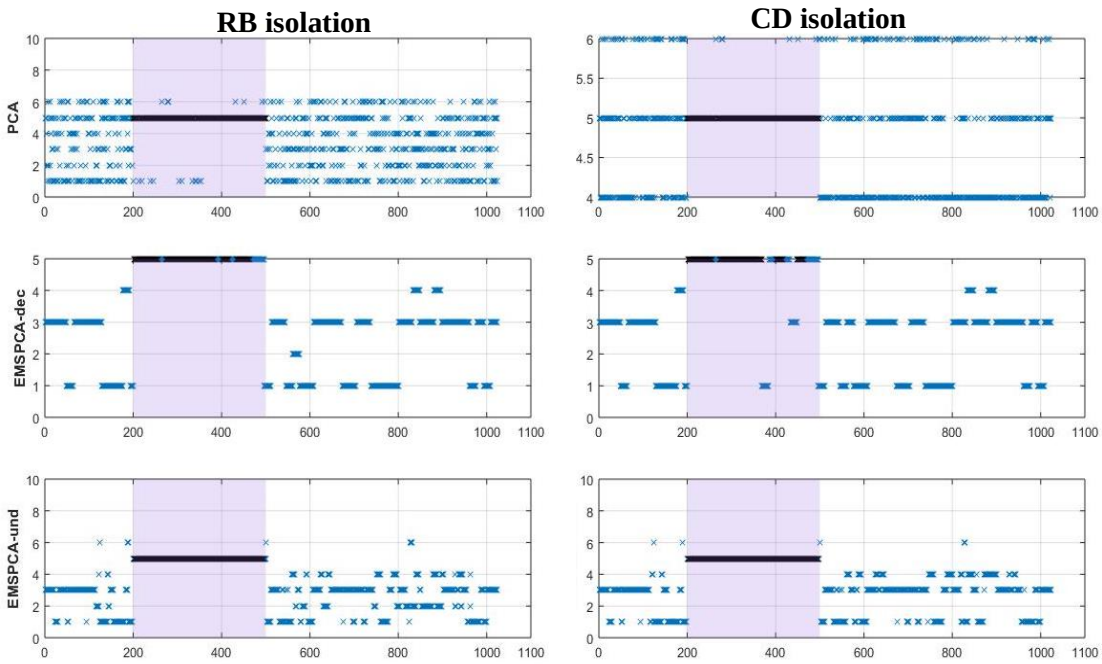

Figure 30: TEP stripper RB and CD isolation results.

As seen in Table 8, the RB FIR for PCA is improved by both the decimated and the undecimated EMSPCA method. However, the CD FIR for PCA is worse when using decimated EMSPCA and better when using undecimated MSPCA. This drop in FIR performance when using EMSPCA can be due to multiple reasons including the lower DR and the lower number of PC that was used to build the model. From Figure 30, it is observed how smearing is reduced significantly with the undecimated EMSPCA method.

5. PACKED-BED PILOT PLANT APPLICATION

This section will validate the proposed FDI algorithm with a real example where no priori assumptions are made with the data. Temperature data is obtained from a packed-bed (PB) pilot plant in Texas A&M Qatar, Chemical Engineering Department. The packed column is 6 inches in diameter, 20 feet tall, with a Koch-Sulzer structured packing. The pilot plant also contains a total condenser, forced circulation reboiler, 4 pumps, and 5 heat exchangers. A DeltaV DCS with 7 different control loops is used to control the column. A process flow diagram of the pilot plant is shown in Figure 31, modified from Texas A&M's CHEN 433 Lab Manual [61].

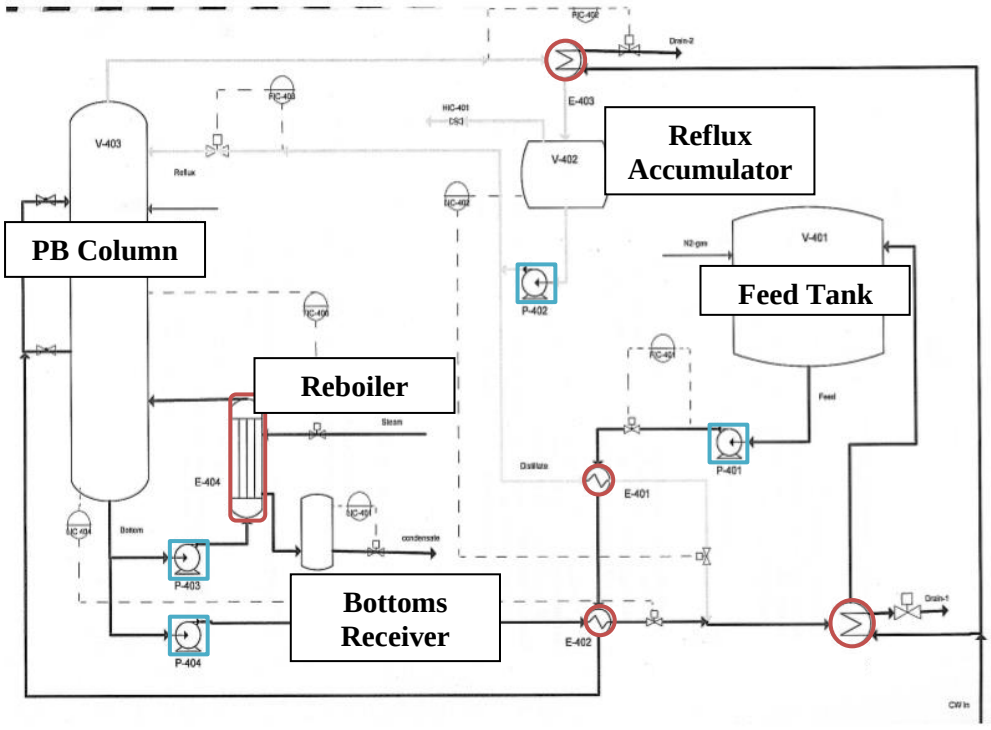

Figure 31: Packed bed pilot plant process flow diagram (adapted [61]).

A total of 12 temperature variables are used in this analysis, where 4 temperature sensors are located along the PB column, and the remaining sensors measure the temperatures at: the column top, the distillate product, bottom product, cooling water inlet, cooling water outlet, solvent temperature, and 2 feed inlets. The fault was arbitrarily chosen to be added to variable 1 (inlet feed temperature) from sample 500 to 800. The original data and the faulty data are illustrated in Figure 32.

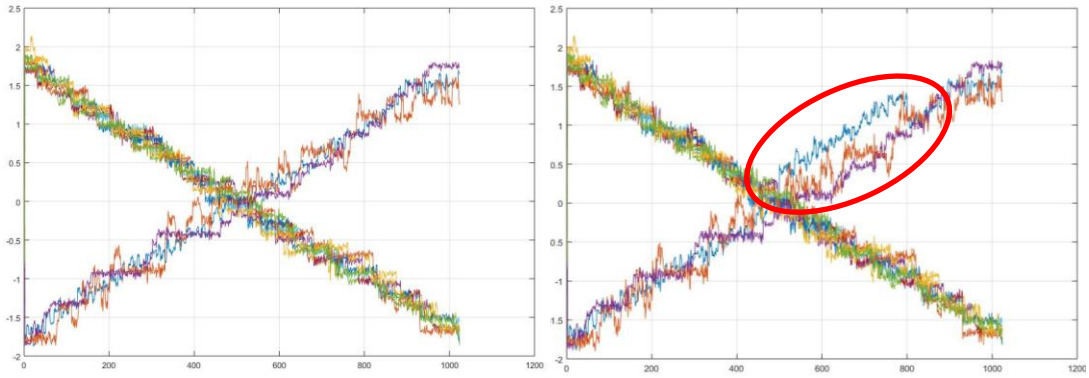

Figure 32: Training (left) and testing data (left) for pilot plant.

For this study, a CPV of 95% was used to determine the number of PCs, a decomposition depth of 3 is used, the theoretical limit of 99% was used to threshold the detail signals, and a 95% empirical limit was used for the reconstructed time domain signal.

5.1. Pilot Plant Detection Results

The detection results for the traditional PCA, conventional MSPCA, and Enhanced MSPCA are illustrated in Figure 33 and summarized in Table 9.

Table 9: Pilot plant application detection results.

Method	#PCs	DR %	FAR %
PCA	1	73.754	3.3195
MSPCA (dec)	1	13.621	1.5214
MSPCA (und)	1	26.578	2.3513
EMSPCA (dec)	1	84.718	3.0429
EMSPCA (und)	1	92.027	2.7663

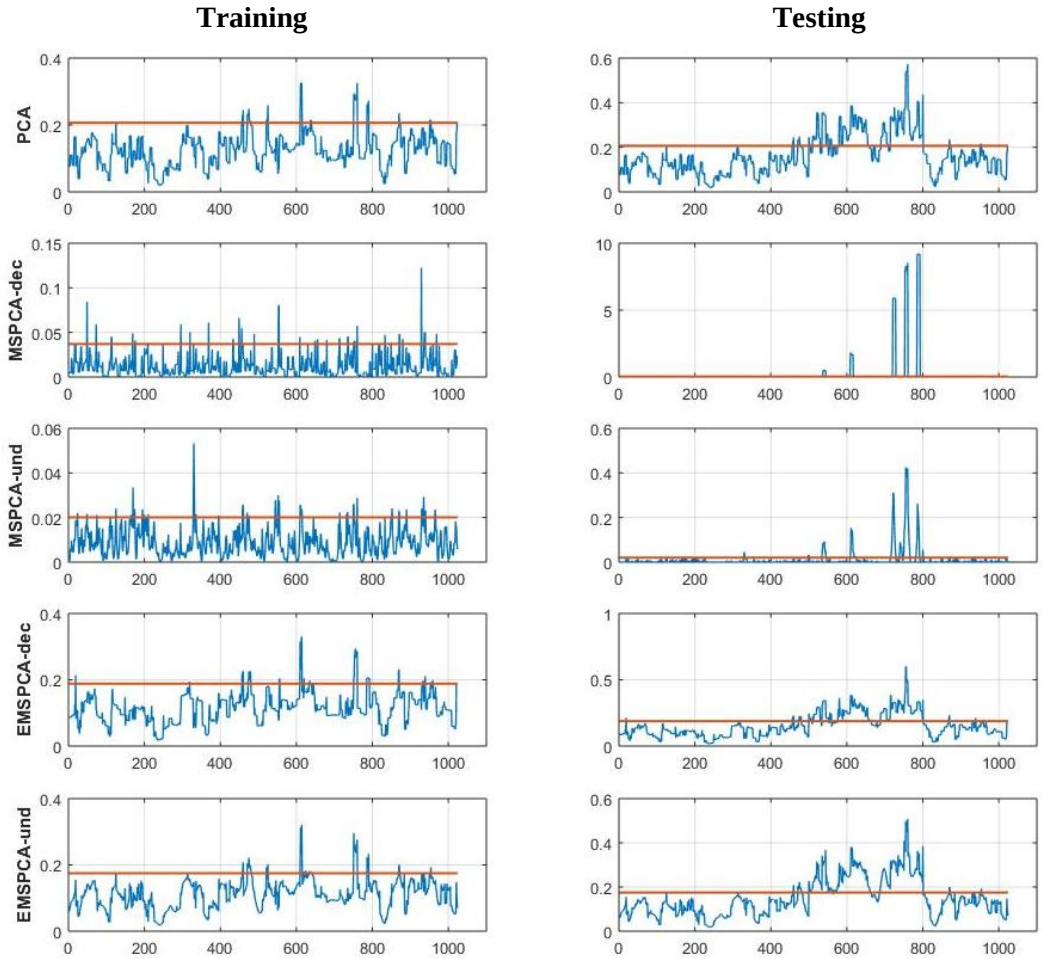

Figure 33: Pilot plant Q-statistic detection results.

In this example, the conventional MSPCA method has a poor detection performance with 13.6% and 26.6% DRs. MSPCA discards the approximate signal in the training data (as per the selection criteria) which leads to a bad PCA model that fails to project the testing data onto the residual subspace where the Q statistic is able to detect the fault (see the testing data Q statistic for MSPCA in Figure 33).On the other hand, Table 9 indicates that the undecimated and decimated EMSPCA approaches have a significantly better DR when compared to traditional PCA (despite comparable FARs).

5.2. Pilot Plant Isolation Results

The isolation results for the Pilot Plant temperature data are summarized in Table 10.

Table 10: Pilot plant isolation results.

Method	**FIR-RB %**	**FIR-CD %**
PCA	95.0	95.0
EMSPCA (dec)	98.0	98.0
EMSPCA (und)	98.9	98.9

As indicated in Table 10, the undecimated EMSPCA has the best RB and CD isolation performance with a 98.9% FIR. It is about 4% better than the traditional PCA method. This improvement is due to multiscale's ability to separate stochastic and deterministic features which reduce the smearing that causes incorrect isolations. The undecimated EMSPCA is about 1% better that the decimated EMSPCA, which suggests that the mode of decomposition does not impact the FIR as much as it does DR.

When comparing the RB and CD isolation approaches, it is apparent that both perform equally for all listed methods in the table, even though the RB approach is theoretically expected to perform better. This is because, in this specific example, only 1 principal component was used to build the PCA model. Consequently, smearing becomes less of an issue, as each variable is equally projected onto the residual subspace (i.e. all variables are weighted by a similar c coefficient value). Regardless, the EMSPCA algorithm demonstrates better isolation performance for both approaches (RB and CD) for data from a real process application. Figure 34 below illustrates the isolation results, where the faulty variable which was correctly detected and isolated is in black while the other points are in blue. The faulty region is patched in purple.

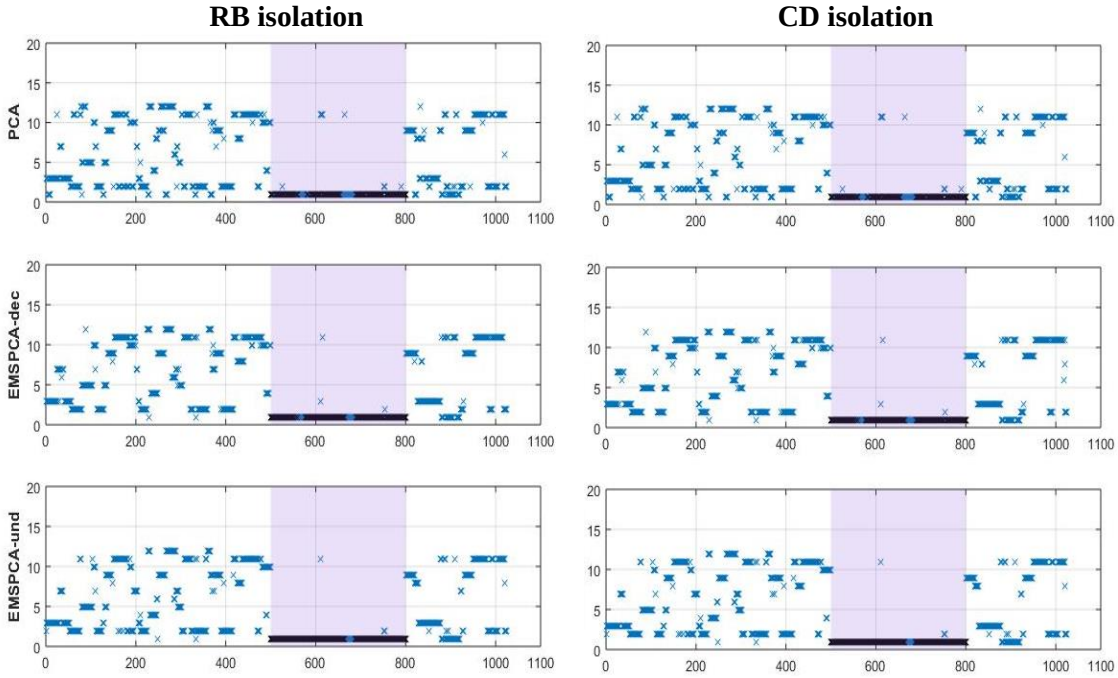

Figure 34: Pilot plant RB and CD isolation results.

6. CONCLUSION

6.1. Conclusion

This work proposes a fault detection and isolation algorithm that uses EMSPCA and recommends the reconstruction-based approach to improve detection and isolation performance. The EMSPCA algorithm modifies the coefficient selection rules implemented by conventional MSPCA to improve the detection rate, and utilizes soft-thresholding of testing details to reduce the false alarm rate. The Monte Carlo simulations indicated that EMSPCA is able to generate more dependable detection limits for a wider range of fault projections. As a result, EMSPCA consistently outperformed the conventional MSPCA algorithm in terms of detection performance, for small and moderate fault sizes and across most depths. The EMSPCA's superior detection performance was also successfully validated by the pilot plant and TEP applications.

Moreover, the results highlight how EMSPCA reduces the effects of smearing on the isolation rate for both reconstruction based (RB) and complete decomposition (CD) isolation methods. EMSPCA isolation was generally a lot better than PCA isolation for both the synthetic and real data applications. Largest improvements in isolation rate was shown for relatively small faults where noise smearing had the largest interference. The Monte Carlo simulations also demonstrate that the reconstruction-based isolation performed significantly better than complete decomposition isolation across all the fault sizes; Reconstruction based methods reached 100% FIR for a large enough fault while the contribution plots plateaued at a value less than 100%. However, when the RB and CD

methods were tested on the TEP stripper unit and the packed bed pilot plant data, they were found to perform the same. Finally, it was consistently evident that the undecimated wavelet transform provides valuable data redundancy which improve detection and isolation performances when compared with the decimated wavelet transform.

6.2. Future Directions

For future directions it is recommended to,

- Test multivariable faults, process faults, and different types of sensor faults (i.e. precision degradation and drifting).
- Use MS analysis with nonlinear data detection isolation techniques (i.e. kernel PCA).
- Test the reliability of the proposed algorithm for different confidence levels and for different detection statistics (T^2 and φ).

REFERENCES

[1] B. Marr, “What Everyone Must Know About Industry 4.0,” *Forbes*, Jun-2016. [Online]. Available: https://www.forbes.com/sites/bernardmarr/2016/06/20/what-everyone-must-know-about-industry-4-0/#fc0b48795f7f.

[2] R. Bharaqwaj, “Machine Learning in the Chemical Industry-BASF, DOW, Royal Dutch Shell, and More,” *Emerj*, Feb-2019. [Online]. Available: https://emerj.com/ai-sector-overviews/machine-learning-chemical-industry-basf-dow-shell/.

[3] I. Nimmo, “Adequately address abnormal operations,” *Chem. Eng. Prog.*, vol. 91, p. 9, 1995.

[4] M. Thirumarimurugan, N. Bagyalakshmi, and P. Paarkavi, “Comparison of fault detection and isolation methods: A review,” in *2016 10th International Conference on Intelligent Systems and Control (ISCO)*, 2016, pp. 1–6.

[5] D. Miljković, “Fault detection methods: A literature survey.,” in *2011 Proceedings of the 34th International Convention MIPRO*, 2011, pp. 750–755.

[6] R. Dunia and S. Joe Qin, “A unified geometric approach to process and sensor fault identification and reconstruction: The unidimensional fault case,” *Comput. Chem. Eng.*, vol. 22, no. 7–8, pp. 927–943, 1998.

[7] J.-M. Lee, C. Yoo, S. W. Choi, P. A. Vanrolleghem, and I.-B. Lee, “Nonlinear process monitoring using kernel principal component analysis,” *Chem. Eng. Sci.*, vol. 59, no. 1, pp. 223–234, 2004.

[8] B. Bakshi, “Multiscale PCA with application to multivariate statistical process monitoring,” *AIChE J.*, vol. 44, no. 7, pp. 1596–1610, Jul. 1998.

[9] S. Wold, “Exponentially weighted moving principal components analysis and projections to latent structures,” *Chemom. Intell. Lab. Syst.*, vol. 23, no. 1, pp. 149–161, 1994.

[10] R. GANESAN, T. K. DAS, and V. VENKATARAMAN, “Wavelet-based multiscale statistical process monitoring: A literature review,” *IIE Trans.*, vol. 36, no. 9, pp. 787–806, Sep. 2004.

[11] M. Misra, H. H. Yue, S. J. Qin, and C. Ling, "Multivariate process monitoring and fault diagnosis by multi-scale PCA," *Comput. Chem. Eng.*, vol. 26, no. 2002, pp. 1281–1293, 2002.

[12] S. N. S. Mirin and N. A. Wahab, "Fault detection and monitoring using multiscale principal component analysis at a sewage treatment plant," *J. Teknol.*, vol. 3, no. 3, pp. 87–92, 2014.

[13] M. Z. Sheriff, M. Mansouri, M. N. Karim, H. Nounou, and M. Nounou, "Fault detection using multiscale PCA-based moving window GLRT," *J. Process Control*, vol. 54, pp. 47–64, 2017.

[14] S. Yoon and J. F. MacGregor, "Unifying PCA and multiscale approaches to fault detection and isolation," *IFAC Proc. Vol.*, vol. 34, no. 25, pp. 433–438, 2001.

[15] A. Lachouri, K. Baiche, R. Djeghader, N. Doghmane, and S. Oulitati, "Analyze and fault diagnosis by multi-scale PCA," *2008 3rd Int. Conf. Inf. Commun. Technol. From Theory to Appl. ICTTA*, 2008.

[16] H. Zhang and Y. Wang, "Improved MSPCA with application to process monitoring," in *2006 International Technology and Innovation Conference (ITIC 2006)*, 2006, pp. 2257–2261.

[17] S. Yoon and J. F. MacGregor, "Principal-component analysis of multiscale data for process monitoring and fault diagnosis," *AIChE J.*, vol. 50, no. 11, pp. 2891–2903, 2004.

[18] S. Yoon and J. F. MacGregor, "Fault diagnosis with multivariate statistical models part I: Using steady state fault signatures," *J. Process Control*, vol. 11, no. 4, pp. 387–400, 2001.

[19] B. Mnassri, E. M. El Adel, and M. Ouladsine, "Reconstruction-based contribution approaches for improved fault diagnosis using principal component analysis," *J. Process Control*, vol. 33, pp. 60–76, 2015.

[20] C. Alcala and S. J. Qin, "Reconstruction-based contribution for process monitoring," in *IFAC Proceedings Volumes (IFAC-PapersOnline)*, 2008, vol. 17, no. 1 PART 1.

[21] H. Burrus, C. Sidney,. Gopinath, Ramesh,. Guo, "Orthogonal Wavelets via Filter Banks Theory and Applications," *Rice Univ. Houston, Texas*, p. 281, 2000.

[22] L. I. Smith, “A tutorial on principal components analysis,” 2002.

[23] R. Dunia, S. J. Qin, T. F. Edgar, and T. J. McAvoy, “Identification of Faulty Sensors Using Principal Component Analysis,” *AIChE J.*, vol. 42, no. 10, pp. 2797–2811, 1996.

[24] S. J. Qin, “Data-driven Fault Detection and Diagnosis for Complex Industrial Processes,” *IFAC Proc. Vol.*, vol. 42, no. 8, pp. 1115–1125, 2009.

[25] J. E. Jackson, *A user’s guide to principal components*, vol. 587. John Wiley & Sons, 2005.

[26] H. T. Eastment and W. J. Krzanowski, “Cross-Validatory Choice of the Number of Components from a Principal Component Analysis,” *Technometrics*, vol. 24, no. 1, pp. 73–77, 1982.

[27] W. J. Krzanowski, “Cross-validatory choice in principal component analysis; some sampling results,” *J. Stat. Comput. Simul.*, vol. 18, no. 4, pp. 299–314, Jan. 1983.

[28] C. F. Alcala and S. Joe Qin, “Analysis and generalization of fault diagnosis methods for process monitoring,” *J. Process Control*, vol. 21, no. 3, pp. 322–330, 2011.

[29] C. F. Alcala and S. Joe Qin, “Analysis and generalization of fault diagnosis methods for process monitoring,” *J. Process Control*, vol. 21, no. 3, pp. 322–330, 2011.

[30] R. Dunia, F. Systems, S. J. Qin, T. F. Edgar, and T. J. Mcavoy, “Identification of Faulty Sensors Using Principal Component Analysis,” *Process Syst. Eng.*, vol. 42, no. 10, pp. 2707–2812, 1996.

[31] J. E. Jackson, “Quality Control Methods for Several Related Variables,” *Technometrics*, vol. 1, no. 4, pp. 359–377, 1959.

[32] J. E. Jackson and G. S. Mudholkar, “Control Procedures for Residuals Associated with Principal Component Analysis,” *Technometrics*, vol. 21, no. 3, pp. 341–349, 1979.

[33] H. Hotelling, “Analysis of a complex of statistical variables into principal components,” *J. Educ. Psychol.*, vol. 24, no. 7, pp. 498–520, Oct. 1933.

[34] J. E. Jackson, “Quality Control Methods for Several Related Variables,” *Technometrics*, vol. 1, no. 4, pp. 359–377, 1959.

[35] H. H. Yue and S. J. Qin, “Reconstruction-based fault identification using a combined index,” *Ind. Eng. Chem. Res.*, vol. 40, no. 20, pp. 4403–4414, 2001.

[36] M. Z. Sheriff and M. N. Nounou, “Improved Fault Detection and Process Safety Using Multiscale Shewhart Charts.,” *J. Chem. Eng. Process Technol.*, vol. 08, no. 02, 2017.

[37] N. Kehtarnavaz and N. Kim, “Chapter 7 - Frequency Domain Processing,” N. Kehtarnavaz and N. B. T.-D. S. P. S.-L. D. U. L. Kim, Eds. Burlington: Newnes, 2005, pp. 139–145.

[38] C. Perrin, B. Walczak, and D. Luc Massart, *The Use of Wavelets for Signal Denoising in Capillary Electrophoresis*, vol. 73. 2001.

[39] C. Valens, *A Really Friendly Guide to Wavelets*. 2000.

[40] R. K. Young, *Wavelet Theory and Its Applications*. Kluwer Academic, 1993.

[41] H. N. Nounou and M. N. Nounou, “Multiscale fuzzy Kalman filtering,” *Eng. Appl. Artif. Intell.*, vol. 19, no. 5, pp. 439–450, 2006.

[42] P. Miller, R. E. Swanson, and C. F. Heckler, “Contribution plots: The missing link in multivariate quality control,” *Fall Conf. ASQC ASA*, 1993.

[43] B. M. Wise, N. B. Gallagher, R. Bro, J. M. Shaver, W. Winding, and R. S. Koch, “No Title,” *PLS Toolbox User Man.*, 2006.

[44] P. Nomikos and J. F. MacGregor, “Multivariate SPC charts for monitoring batch processes,” *Technometrics*, vol. 37, no. 1, pp. 41–59, 1995.

[45] T. Kourti and J. F. MacGregor, “Multivariate SPC Methods for Process and Product Monitoring,” *J. Qual. Technol.*, vol. 28, no. 4, pp. 409–428, Oct. 1996.

[46] S. Wang and F. Xiao, “Detection and diagnosis of AHU sensor faults using principal component analysis method,” *Energy Convers. Manag.*, vol. 45, no. 17, pp. 2667–2686, 2004.

[47] D. Xiao, X. Gao, J. Wang, and Y. Mao, “Process Monitoring and Fault Diagnosis for Shell Rolling Production of Seamless Tube,” *Hindawi*, no. Mathematical Problems in Engineering, p. 12, 2015.

[48] R. Dunia, S. J. Qin, T. F. Edgar, and T. J. McAvoy, “Identification of Faulty Sensors Using Principal Component Analysis,” *AIChE J.*, vol. 42, no. 10, pp. 2797–2811, 1996.

[49] C. F. Alcala and S. J. Qin, “Reconstruction-based contribution for process monitoring,” *Automatica*, vol. 45, no. 7, pp. 1593–1600, 2009.

[50] A. Raich and A. Çinar, “Statistical Process Monitoring and Disturbance Diagnosis in Multivariable Continuous Processes,” *AIChE J.*, vol. 42, no. 4, pp. 995–1009, 1996.

[51] R. Dunia, S. Joe Qin, T. F. Edgar, and T. J. McAvoy, “Use of principal component analysis for sensor fault identification,” *Comput. Chem. Eng.*, vol. 20, pp. S713–S718, 1996.

[52] P. Van Den Kerkhof, J. Vanlaer, G. Gins, and J. F. M. Van Impe, “Analysis of smearing-out in contribution plot based fault isolation for Statistical Process Control,” *Chem. Eng. Sci.*, vol. 104, pp. 285–293, 2013.

[53] C. F. Alcala and S. J. Qin, “Reconstruction-based contribution for process monitoring,” *Automatica*, vol. 45, no. 7, pp. 1593–1600, 2009.

[54] J. Liu, “Fault diagnosis using contribution plots without smearing effect on non-faulty variables,” *J. Process Control*, vol. 22, no. 9, pp. 1609–1623, 2012.

[55] H. Ji, X. He, and D. Zhou, “On the use of reconstruction-based contribution for fault diagnosis,” *J. Process Control*, vol. 40, pp. 24–34, 2016.

[56] J. Wang, W. Ge, J. Zhou, H. Wu, and Q. Jin, “Fault isolation based on residual evaluation and contribution analysis,” *J. Franklin Inst.*, vol. 354, no. 6, pp. 2591–2612, 2017.

[57] C. Alcala and S. J. Qin, “Reconstruction-based contribution for process monitoring,” in *IFAC Proceedings Volumes (IFAC-PapersOnline)*, 2008, vol. 17, no. 1 PART 1.

[58] L. H. Chiang, E. L. Russell, and R. D. Braatz, “Tennessee Eastman Process BT - Fault Detection and Diagnosis in Industrial Systems,” L. H. Chiang, E. L. Russell, and R. D. Braatz, Eds. London: Springer London, 2001, pp. 103–112.

[59] P. R. Lyman and C. Georgakis, “Plant-wide control of the Tennessee Eastman problem,” *Comput. Chem. Eng.*, vol. 19, no. 3, pp. 321–331, 1995.

[60] A. Bathelt, N. L. Ricker, and M. Jelali, “Revision of the Tennessee Eastman Process Model,” *IFAC-PapersOnLine*, vol. 48, no. 8, pp. 309–314, 2015.

[61] “Chemical Engineering Unit Operations Laboratory II CHEN 433.” Texas A&M University at Qatar, p. 165, 2019.